JOURNAL OF COASTAL AND HYDRAULIC STRUCTURES

Vol. 1, 2021, 10

Standing wave impacts on vertical hydraulic structures with overhangs for varying wave fields and configurations

Ermano de Almeida[1] and Bas Hofland[2]

Abstract

This study focuses on standing wave impacts on vertical hydraulic structures with relatively short overhangs. It addresses the demand for extended knowledge and loading prediction expressions for these structures. Based on laboratory experimental data from 146 tests, this paper works on two complementary objectives. Firstly, this study extends the knowledge on this type of wave impact addressing the following aspects: changes in hydraulic loading conditions (regular/irregular waves and varying freeboards) and changes in the structure geometry (lateral constriction and loading reducing ventilation gaps). All laboratory tests consider relatively short overhangs, with ratios of wave length to overhang length between 10 and 40, and ratios of overhang height to overhang length of 3 and 6. The regular wave tests showed that the tests with the longer overhang were related to longer impact durations and larger loading variability compared to the tests with the shorter overhang. Also, tests with reduced freeboards produced larger impact loads. In addition, repeated tests presented equal impulse values (I, β, t_d, Λ). Furthermore, the pressure peaks measured at one location were found to not represent the pressure peaks averaged over the structure width, while the pressure-impulses measured at one location were found to properly represent the pressure-impulses averaged over the width. The constriction tests showed that a lateral constriction amplifies pressure peaks and pressure-impulses at the constriction edge. The ventilation gap tests showed that ventilation gaps are effective in reducing force peaks and force-impulses. The irregular wave tests highlighted that the dynamic interactions of the incident waves with the structural configurations are even more dynamic and variable in tests with irregular wave conditions. Secondly, this study presents loading prediction expressions for preliminary loading estimations built up by the previously developed pressure-impulse theory that is empirically calibrated using the presently acquired experimental data. To that end, the relation between the effective bounce-back factor $(1 < \beta < 2)$ with the Gamma Parameter (Γ) is described. These loading prediction expressions may be used for preliminary load estimations and in combination with structural response models.

Keywords:

wave impacts, hydraulic structures, impulsive loading, overhangs

[1]E.deAlmeida@tudelft.nl, Delft University of Technology, Delft, The Netherlands
[2]B.Hofland@tudelft.nl, Delft University of Technology, Delft, The Netherlands

This paper was submitted 11 July 2021. It was accepted after double-blind review on 27 November 2021 and published online on 24 December 2021"

DOI: https://doi.org/10.48438/jchs.2021.0010

Cite as: "De Almeida, E., Hofland, B. Standing wave impacts on vertical hydraulic structures with overhangs for varying wave fields and configurations. Journal of Coastal and Hydraulic Structures, 1, p.10. https://doi.org/10.48438/jchs.2021.0010"

The Journal of Coastal and Hydraulic Structures is a community-based, free, and open access journal for the dissemination of high-quality knowledge on the engineering science of coastal and hydraulic structures. This paper has been written and reviewed with care. However, the authors and the journal do not accept any liability which might arise from use of its contents.

1 Introduction

During the coming years and decades, numerous hydraulic structures will be constructed worldwide. Also, various existing hydraulic structures will be renovated after reaching the end of their design lifetime or due to increasing safety standards and/or loading conditions. Figure 1 shows one of such singular hydraulic structures, the flood gate complexes in the Afsluitdijk in The Netherlands. The Afsluitdijk is currently being fully renovated after almost 90 years of operation. The renovation of the Afsluitdijk includes the complete renewal of the existing flood gate complexes, and the construction of additional flood gate complexes to cope with sea level rise and more extreme weather scenarios. Such construction and renovation projects require the development of design guidelines and prediction methods for determining wave impact characteristics and magnitudes.

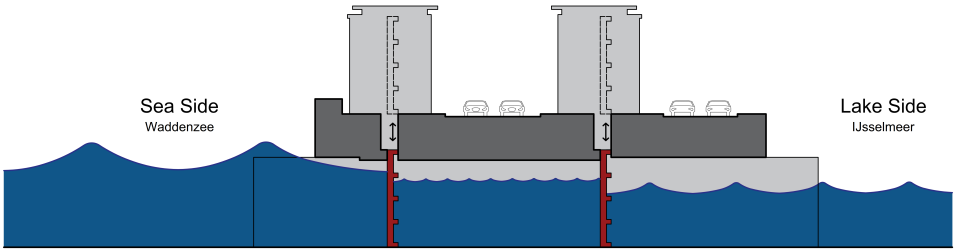

Figure 1: Existing Afsluitdijk flood gate, during high water at the sea side (de Almeida and Hofland, 2020*a*).

Three types of wave impacts are described in de Almeida and Hofland (2020*a*): breaking waves acting on a vertical wall, overtopping waves acting on a crest wall and non-breaking waves acting on a vertical wall with a horizontal overhang. This study focuses on this third type of wave impact (i.e. standing wave impacts on vertical structures with overhangs). This type of wave impact is determinant for structures as shown in Figure 1, but also for many others such as crest walls, lock gates, sluice gates, dewatering sluices, flood gates and storm surge barriers. Until recently, only a few studies were conducted on wave impact loads acting on vertical hydraulic structures with overhangs (Ramkema, 1978; Kisacik et al., 2014). Nevertheless, this wave impact type is gaining increasing attention in the past years. Recent developments on the study of standing wave impacts on hydraulic structures were presented by Castellino et al. (2018), Martinelli et al. (2018), de Almeida and Hofland (2020*a*), de Almeida and Hofland (2020*b*), Castellino et al. (2021) and Dermentzoglou et al. (2021), among others. Furthermore, recent studies have also addressed wave impacts on overhang configurations that occur in nature, for example on cliffs and shore platforms (Renzi et al., 2018).

Bagnold (1939) contributed to the study of impulsive loading caused by breaking waves, including two key findings. Firstly, the highest pressure magnitudes were measured when the air cushion between the wave front and the impact surface was small, but not zero. Secondly, although maximum peak pressures present large fluctuations, the area enclosed by the pressure-time curve (i.e. the pressure-impulse P) was remarkably constant. Further research on impulsive loadings caused by wave impacts has mainly focused on breaking wave impacts on vertical structures (Minikin, 1950; Goda, 1974; Takahashi et al., 1994; Oumeraci et al., 2001; Cuomo et al., 2010). In addition, breaking wave impacts have also been studied for structures with relatively long overhangs (Kisacik et al., 2014). Regarding overtopping wave impacts, this wave impact type has also been studied recently by Chen et al. (2015, 2016).

A comprehensive series of laboratory tests took place in The Netherlands for the design and construction of the Delta Works (1953-1997). A large number of those laboratory tests focussed on wave impact loadings on the Eastern Scheldt Storm Surge Barrier, including standing wave impacts in configurations with overhangs (Ramkema, 1978; WL, 1977, 1978). However, those studies focussed on design optimization and scaling laws and did not introduce general design criteria for such types of hydraulic structures. More recently, Hofland (2015) studied impulsive wave impact loading acting on the existing Afsluitdijk flood gates, including the effect of the existing overhang and ventilation gap. Nevertheless, those tests were once more focused on representing a particular structural configuration and did not introduce general design guidelines.

The pressure-impulse theory applied to wave impacts was first presented by Cooker and Peregrine (1990, 1995). This theoretical model allows calculating the pressure-impulse caused by a wave impact and was developed based on the Navier-Stokes equations of motion. This theory was first presented considering a horizontally moving volume of water (describing a simplified breaking wave) impacting on a vertical wall. Later on, Wood and Peregrine (1996) extended this theory considering a vertically moving volume of water (describing a simplified

reflecting wave) impacting on a horizontal overhang. This theory was validated by de Almeida and Hofland (2020*a*), combining the models from Cooker and Peregrine (1990, 1995) and Wood and Peregrine (1996). This validation was done for a vertical wall with a horizontal overhang subjected to standing incident waves and obtained a close confirmation of the theory. The advantages of using the pressure-impulse and force-impulse for preliminary load estimations instead of pressure and force peaks were presented by Chen et al. (2019). Furthermore, a model to estimate reaction forces from impulsive wave impact loads was also introduced. Tieleman et al. (2019, 2021) developed a semi-analytical model for predicting the bending vibrations of vertical hydraulic structures subjected to impulsive wave impact loadings, including the configuration of a vertical wall with a horizontal overhang (e.g. flood gates shown in red in Figure 1).

Various authors have focussed on the study of impulsive wave loads on recurved crest walls on vertical breakwaters (Castellino et al., 2018, 2021; Martinelli et al., 2018; Dermentzoglou et al., 2021). Those authors have addressed both the loading and response aspects, considering both experimental and numerical methods. In addition to de Almeida and Hofland (2020*a*), de Almeida and Hofland (2020*b*) has also studied standing wave impacts with a focus on the wave impact velocity and entrapped air characteristics. There, the details of the entrapped air and the kinematics of the impacting wave surface were seen to determine the impact duration. This study confirmed the observations from WL (1979), which highlighted that the presence of air pockets has a decisive effect on the characteristics and magnitudes of wave impact loadings. Wave impact loads acting on similar structures such as piers and bridge decks were also studied recently (McConnell et al., 2004; Cuomo et al., 2007; Seiffert et al., 2014; Hayatdavoodi et al., 2014). In addition, other studies present recent experimental and numerical models and tools for assessing slamming loads on offshore structures, natural gas tanks and ship hulls (Dias and Ghidaglia, 2018; Sonneville et al., 2015; Bogaert, 2018). Those contributions show that, besides significant differences, common processes are observed in confined wave impacts in hydraulic structures, piers, bridge decks, offshore structures/platforms and during sloshing impacts inside gas tankers. One key difference is that de Almeida and Hofland (2020*a*) has focused on describing the confined wave impact load by the pressure/force-impulse based on regular wave laboratory tests and the pressure-impulse theory. This is different to many other studies that focused on describing wave impact loads mostly in terms of pressure/force peaks. Thus, a knowledge gap still exists in describing confined wave impact loads on realistic configurations loaded by irregular wave fields considering the pressure/force-impulses and based on the pressure-impulse theory.

The previously described literature presented a range of contributions on wave impacts in general and confined wave impacts in particular. Nevertheless, important knowledge gaps remain in the study of standing wave impacts on vertical hydraulic structures with relatively short overhangs. Mainly, there is a lack of loading prediction expressions for this type of wave impact. Knowledge gaps also exist on the influence of irregular incident waves, the effect of different water levels, the spatial distribution of loading and load reducing ventilation gaps. This paper addressed those knowledge gaps, based on experimental data and the pressure-impulse theory.

The aims of this paper are divided into two objectives. Firstly, to extend the knowledge on this type of wave impact addressing the following four aspects: regular and irregular incident waves, the effect of different water levels, the spatial distribution of loading in configurations with and without realistic geometrical variations like lateral constrictions and load reducing ventilation gaps. Secondly, to present loading prediction expressions for preliminary loading estimations based on laboratory experimental data and the pressure-impulse theory. Section 2 describes the theoretical expressions used in this study. Section 3 describes the setup, characteristics and configurations of the laboratory experiments. Section 4 presents all experimental results, including the loading prediction expressions based on laboratory experimental data and the pressure-impulse theory. Section 5 discusses the main aspects of this work, while Section 6 summarizes the main conclusions of this study.

2 Theoretical methods

This section summarizes the most important theoretical expressions and concepts used in this study. It includes the main expressions of the pressure-impulse theory, the estimation of the wave impact velocity based on linear wave theory and the characteristics of the Rayleigh distribution. Figure 2 describes the main hydraulic and structural parameters used in this study. Furthermore, the pressure-impulse expression is shown in Equation 1.

$$P = \int_{t_d} p \, dt \tag{1}$$

where P [Pa s] is the pressure-impulse, p [Pa] is the pressure and t_d [s] is the impact duration.

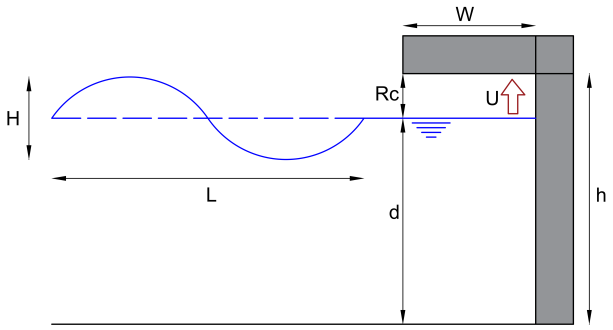

Figure 2: Hydraulic and structural parameters: incident wave height H [m]; incident wave length L [m]; still water depth d [m]; overhang height h [m], overhang width W [m]; freeboard R_c [m]; impact velocity U [m/s].

Pressure-impulse theory

In this paper, the pressure-impulse model is used in a dimensionless form, as presented by Wood and Peregrine (1996) and validated in de Almeida and Hofland (2020*a*). The dimensionless model is obtained by considering the overhang length W as the geometric scaling magnitude. This is justified by the fact that the overhang length W is the length over which the vertically-moving water surface impacts the horizontal overhang. Then, W is used for obtaining the dimensionless geometric magnitudes, such as the dimensionless overhang length ($\bar{W} = 1$) and the dimensionless overhang height ($\bar{h} = h/W$). For the conversion between dimensionless and dimensional impulse results, Equations 2 and 3 are used. Equation 2 is used for the pressure-impulse P obtained at any point in the fluid domain. Equation 3 is used for the total force-impulse I integrated over a given boundary, such as the vertical wall that extends from beneath the overhang to the bottom. In these equations and throughout this study, the overbar sign "$^-$" represents dimensionless values.

$$\bar{P} = \frac{P}{\rho U W} \tag{2}$$

$$\bar{I} = \frac{I}{\rho U W^2} \tag{3}$$

where ρ [kg/m^3] represents the fluid density and U [m/s] represents the wave impact velocity.

A summary of the validated pressure-impulse theory is presented hereafter. For the detailed theoretical descriptions of the model and full validation process, please refer to de Almeida and Hofland (2020*a*). All three Equations 4-6 shown here were obtained as fits in de Almeida and Hofland (2020*a*) from the analytical model by Wood and Peregrine (1996). The total dimensionless force-impulse $\bar{I}$ applied along the vertical wall can be calculated for any value of dimensionless overhang height $\bar{h}$ and effective bounce-back factor β according to the expression presented in Equation 4. C_I represents the total theoretical dimensionless force-impulse (i.e. $\beta = 1$), obtained as a fit to the pressure-impulse analytical model. Equations 5-6 present the expressions for the maximum (i.e. at the top of the wall) and minimum (i.e. at the bottom of the wall) dimensionless pressure-impulse $\bar{P}$ as function of the dimensionless overhang height $\bar{h}$ and the effective bounce-back factor β. The factor β was introduced by Wood et al. (2000) to describe the increase in impact pressure-impulse due to the bounce-back of entrapped air, with values in the range $1 < \beta < 2$. In this paper, β is used as described in de Almeida and Hofland (2020*a*), to account for all differences between theory and measurement, so it is used as the effective bounce-back factor. From the experimental tests, β is calculated as follows: $\beta = \bar{I}/C_I$. Furthermore, based on Wood et al. (2000), de Almeida and Hofland (2020*a*) introduced the Peregrine Number ($\Lambda = t_d U/W$). This parameter assesses the validity of the pressure-impulse theory. According to Wood et al. (2000) and based on breaking wave impacts, the pressure-impulse theory is applicable for describing wave impacts with lower values of the Peregrine Number ($\Lambda << 1$). The value of $\Lambda = 0.4$ is adopted as an approximate upper limit for the theory validity, while more violent wave impacts with lower values of the Peregrine Number Λ are expected to show better agreement with the pressure-impulse theory.

$$\bar{I} \approx \beta C_I \approx \beta(2\bar{h}^{0.18} - 1.14) \qquad \text{for} \quad 1 \leq \bar{h} \leq 10 \tag{4}$$

$$\bar{P}_{max} \approx \beta(0.18\bar{h}^{-1.9} + 1) \qquad \text{for} \quad 1 \leq \bar{h} \leq 10 \tag{5}$$

$$\bar{P}_{min} \approx \beta(0.75\bar{h}^{-0.97}) \qquad \text{for} \quad 1 \leq \bar{h} \leq 10 \tag{6}$$

Impact velocity

The proposed method to estimate the standing wave impact velocity is linear wave theory. This was used by de Almeida and Hofland (2020*b*) as it is considered suitable for the undisturbed waves within the ranges of steepness and relative depth applied in this study (Hedges, 1995) and it is a well-known theory that can be implemented in future design guidelines. According to this theory, and as presented in the previously mentioned studies, a linear wave reflecting against a vertical wall can be described as in Equation 7.

$$\eta = (1 + cr)\frac{H}{2}\sin\omega t = A_w \sin\omega t \tag{7}$$

where η [m] represents the surface elevation, cr [-] represents the wave reflection coefficient, H [m] represents the incident wave height, ω [rad/s] represents the angular wave frequency ($\omega = 2\pi/T$, where T [s] represents the incident wave period) and A_w [m] represents the total wave amplitude at the wall.

Equation 7 (water surface position) was combined with its derivative (water surface velocity), so the water surface velocity $\dot{\eta}$ is described as function of the water surface position η: $\dot{\eta} = \omega\sqrt{A_w^2 - \eta^2}$ (de Almeida and Hofland, 2020*a*). In addition, a reflection coefficient of $cr = 1$ is used in this method, as the incident wave is not influenced by the presence of the overhang during the period $T/2$ prior to the wave impact. The results presented in de Almeida and Hofland (2020*b*) showed that the wave surface position/velocity estimated with this method is in agreement with the laboratory measurements. A reflection coefficient of $cr = 1$ leads to a total wave amplitude at the wall equal to the incident wave height ($A_w = H$). The wave surface impact velocity U on an overhang with a freeboard ($R_c < H$) can then be obtained from Equation 8.

$$U = \omega\sqrt{H^2 - R_c^2} \tag{8}$$

Rayleigh distribution

For irregular wave fields, the incident wave height of the single waves (H) in Equation 8 should be obtained from the wave field parameters (i.e. significant wave height H_s) and given a certain exceedance probability (i.e. pr). The Rayleigh distribution is used in this study to describe the wave height distribution for a set of given incident wave parameters (Longuet-Higgins, 1952). The Rayleigh distribution is a particular type of Weibull distribution in which the shape parameter is equal to 2. Further, with a scale parameter of 0.5, the cumulative distribution function of the Rayleigh distribution can be re-arranged as in Equation 9. This equation allows obtaining the incident wave heights associated with a given exceedance probability (pr), or a given return period. This can then be used to describe the wave impact velocity of each wave according to Equation 8.

$$H = H_s\sqrt{-\frac{\log(pr)}{2}} \tag{9}$$

3 Laboratory experiments

This section presents the experiments carried out for this study, which includes a total of 146 laboratory tests. This large amount of tests constitutes a robust dataset on this type of wave impact, including a wide range of structural and hydraulic combinations. This experimental dataset is used to draw a wide range of new conclusions and to carry out the validation of the load prediction expressions. Hereafter in this section, the experimental setup, the experiment conditions and the instrumentation are described in more detail.

3.1 Experimental Setup

This study analyses the results of 146 laboratory tests carried out during three test campaigns (2018, 2019, 2020) at the wave flume at the Hydraulic Engineering Laboratory at the Delft University of Technology. Figure 3 illustrates the laboratory test area during the 2019 test campaign. The wave flume used in all tests is 42 m long, 1 m high and 0.8 m wide. The wave generation equipment consists of a piston-type wave maker able to generate regular and irregular waves and is equipped with active reflection compensation (ARC) and second order wave

steering. The test setup was fully built with aluminium elements, supported by a 1500 kg concrete block placed inside the wave flume. This concrete block was 0.8 m wide, 0.8 m long and 1 m high and provided the required stability for the structure subjected to wave impacts. Furthermore, this laboratory model does not represent a precise real structure. It is a schematic configuration, inspired by structures such as the Afsluitdijk sluice gates. For orientation purposes, the dimensions of the laboratory setup would correspond to an approximate 1:15 scale to a structure such as the Afsluitdijk sluice gates. The details on the various structural configurations and test conditions are described in more detail hereafter.

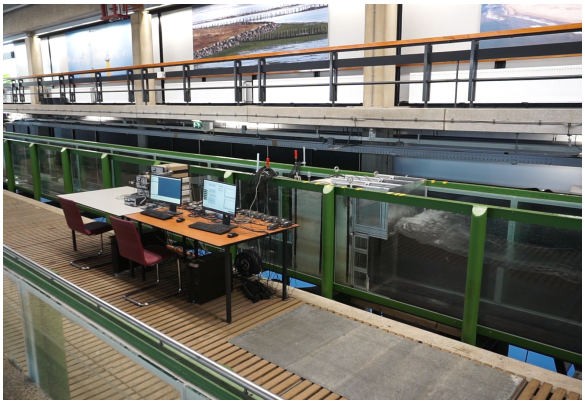

(a) Experimental test area.

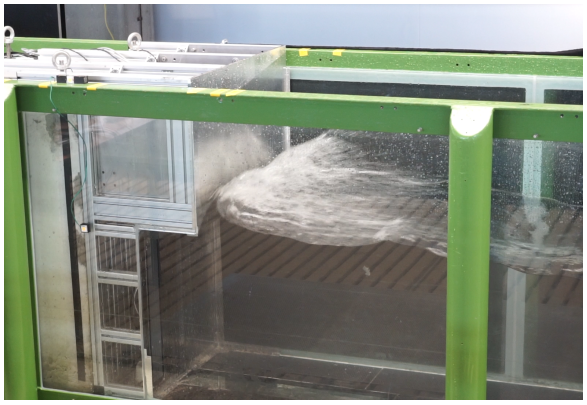

(b) Overhang structure model setup.

Figure 3: Overview of experiments(images taken from de Almeida and Hofland (2020*a*)).

3.2 Experiment Conditions

Table 1 briefly summarizes all laboratory tests used in this study. As shown in Table 1 and Figure 4, three main structural configurations were tested. A common feature of all tests in this study is the constant width of the structure ($M = 0.8$ m) which is equal to the flume width, the constant height of the overhang ($h = 0.6$ m) and the use of two overhang lengths: a shorter overhang "S" ($W = 0.1$ m) and a longer overhang "L" ($W = 0.2$ m). 106 out of the 146 tests were done for the standard configuration, consisting of a vertical wall and a horizontal overhang. For this configuration tests with regular and irregular waves were carried out with variations of wave height (H), wave period (T), wave steepness (s), water depth (d) and freeboard (R_c). This large number of tests fulfilled the goal of allowing a wide range of conclusions on this type of wave impact and providing a robust dataset for the validation of the prediction expressions. Furthermore, two additional configurations were tested, to extend the knowledge on the effects of lateral constrictions and ventilations gaps on the wave impact loads. Those experiments included the remaining 40 tests with only regular waves and a shorter number of variations in the incident wave conditions. More details on the tests carried out (i.e. variations of structural configurations and incident wave conditions) are shown in the Annexes in Table A1.

Table 1: Number of laboratory tests.

Condition	Regular wave	Irregular wave	Total
Standard configuration	54	52	106
Lateral constriction	10	-	10
Ventilation gaps	30	-	30

3.3 Instrumentation

The incident waves parameters were measured at 1.5 metres away from the vertical wall. To this end, an array of three wave gauges with a 100 Hz sampling rate were used, see Figure 4b. Based on the wave gauge measurements, the method from Zelt and Skjelbreia (1992) was used to obtain the incident wave spectra, time-series and parameters (i.e. wave height H and wave period T). These wave gauges were equipped with water conductivity compensation systems to ensure the accuracy of the measurements in all circumstances, adjusting for temperature variations during the tests.

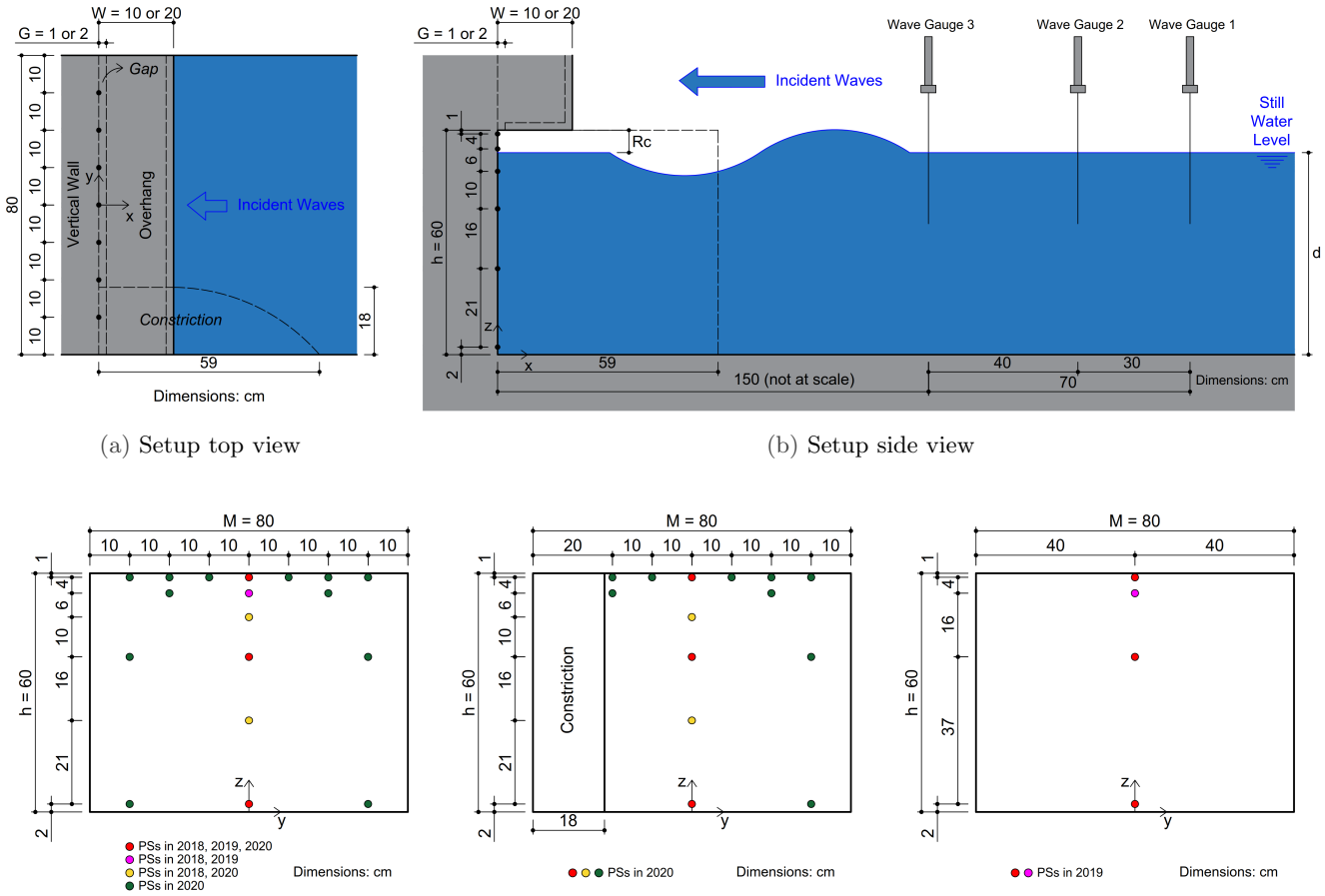

(a) Setup top view

(b) Setup side view

(c) Standard configuration front view

(d) Constriction tests front view

(e) Gap tests front view

Figure 4: Experimental setup characteristics.

Pressures were measured in this study with pressure sensors Kulite HKM-375M-SG with 1 bar measurement range and sealed gauge, screwed flush on the structure aluminium surface. During all tests, a sampling rate of 20 kHz was used for these dynamic pressure measurements. By integrating the pressures measured over the vertical wall, the total forces were obtained. All pressure and force peaks presented throughout this study were calculated from the original unfiltered time series. Furthermore, this study uses the method presented by de Almeida and Hofland (2020*a*) for calculating the pressure-impulses, force-impulses and impact durations generated by the wave impacts. In this method, the original time series is filtered with a low-pass third order Butterworth filter with a cut-off frequency of 100Hz. This cut-off frequency allows to remove higher frequency components but it is sufficiently large to not affect the impulse measurements. Further, the wave impact start is defined as when the pressure becomes larger than zero (i.e. hydrostatic pressure), and the impact end is defined as when the pressure becomes smaller than the quasi-static component. The impact duration (t_d) is then obtained as the time interval between the impact start and the impact end. Next, pressure-impulses are calculated by integrating the pressures between the previously defined impact start and the impact end. Lastly, force-impulses are then calculated by integrating the obtained pressure-impulse profile over the vertical wall height. During the different test campaigns, a different number of pressure sensors (PS) were used: 6 in 2018, 4 in 2019 and 17 in 2020. The locations of these pressure sensors in the three test campaigns are shown in Figures 4c, 4d and 4e for the different test configurations. The calibrations of these pressure sensors obtained at the start of the test campaign were regularly checked during and after the test campaign, with before-after variations in calibration factors around 0.12%. Furthermore, this study uses in all analyses the dynamic values for pressures and forces, which are obtained after the hydrostatic pressure/forces (i.e. the ones measured before wave motion) are removed from the measurements.

4 Experimental results

This section presents and discusses the results of the laboratory experiments. Hereafter, these test results are separated into three parts. Firstly, the results of the regular wave tests with standard configuration are presented. Secondly, the results of the regular wave tests with the non-standard configurations (i.e. lateral constriction and ventilation gaps) are discussed. Lastly, the results of the irregular wave tests are presented.

4.1 Regular wave tests with standard configuration

This experimental set consists of a total of 54 tests, including four water levels, five incident wave conditions and two overhang lengths. Figures 5 and 6 illustrates the regular wave tests with standard configuration, including the combinations of water levels, incident wave conditions and overhang lengths. Here only three test conditions (A, C, E) are presented for simplicity. Nevertheless, these three test conditions (A, C, E) cover the full range of incident wave characteristics and measured wave impact loading. Figure 5 shows the results for the shorter overhang, while Figure 6 shows the results for the longer overhang. These figures show the pressure measurements from the pressure sensor located at the top-centre of the vertical wall ($x = 0$ m, $y = 0$ m, $z = 0.59$ m), see Figure 4c. Detailed results from all the regular wave tests are shown in the Annexes in Table A2.

From Figures 5 and 6, a series of observations can be highlighted. First, for the smallest incident wave condition (rA), no wave impact took place for the highest water level with negative freeboard ($d = 0.63$ m, $R_c = -0.03$ m), see Figures 5d and 6d. This reduces the number of tests with wave impacts in this experimental set to 52, which will be used further in this study. Second, it is observed that repeated tests (for $d = 0.60$ only, see Table A2 for details) showed similar impulsive load characteristics as described by I, β, t_d and Λ. Furthermore, given the reduced values of the Peregrine Number obtained in this study ($\Lambda \leq 0.30$), it is considered that all the tests in this study fall within the range of validity for the pressure-impulse theory (Wood et al., 2000). Third, the tests with longer overhangs presented longer impact durations compared to the tests with shorter overhangs. This can be observed in the results of impact duration (see Table A2 for details) and also visually in Figures 5 and 6. As highlighted in de Almeida and Hofland (2020*b*), this is explained by the fact that a longer overhang is directly related to larger air entrapments and thus directly related to longer impact durations (Mitsuyasu, 1966). In addition, it is also observed that lower water levels are strongly related to shorter impact durations in tests with shorter overhangs. For the tests with longer overhangs this relation between water level and impact duration is less evident but still present. This can be explained by a easier release of the air before wave impacts for lower water levels, leading to shorter impact durations. In the case of higher water levels and reduced freeboards, the air may be more easily entrapped between the wave surface and the structure, leading to longer impact durations. It can then be highlighted that in general the shorter wave impact durations will be expected for shorter overhangs at lower water levels. Fourth, it is also observed that for the same incident wave conditions, the impacts on the longer overhangs (Figure 6) show a more complex and variable behaviour compared to the tests with shorter overhangs (Figure 5). That more complex behaviour for tests with longer overhangs includes frequent vibrations (Figures 6a, 6e, 6i, 6j), pre-peaks (Figures 6b, 6f, 6l), very long impacts (Figures 6b, 6c, 6f, 6g), double peaks (Figure 6k) and even triple peaks (Figure 6h). This higher variability of wave impacts loading characteristics, is driven by the more complex interaction of structural configurations, incident wave conditions and air entrapment in configurations with longer overhangs. For the shorter overhangs, such complex behaviour is still present but less frequent, with less complex wave impact loading characteristics. The majority of tests with the shorter overhang showed a short and high wave impact (Figures 5a, 5b, 5e, 5i, 5j, 5k). Few exceptions include two tests with small vibrations (Figures 5c, 5g), a long impact (Figure 5h), an impact with a short pre-peak (Figure 5l) and a double peak (Figure 5f). Fifth, tests with identical incident wave conditions and different water levels showed a limited variation in the loading curves behaviour, see Figures 5i, 5j and 5k for the shorter overhang or Figures 6e, 6f and 6g for the longer overhang. Sixth, tests with identical water levels and different incident wave conditions showed a limited variation in the loading curves behaviour, see Figures 5a, 5e and 5i for the shorter overhang or Figures 6a, 6e and 6i for the longer overhang. Seventh, the tests with a negative freeboard showed a more complex loading behaviour: pre-peaks (Figures 5l, 6l), long peak (Figure 5h) and a triple peak (Figures 6h).

Figure 7 gives the values of dimensionless total force-impulse $\bar{I}$ obtained from the regular wave tests with standard configuration. This extends the validation of the pressure-impulse theory presented by de Almeida and Hofland (2020*a*), including a larger number of tests (52 tests instead of 14) and also four different water levels (instead of only one). Based on all regular wave tests with standard configuration, the obtained effective

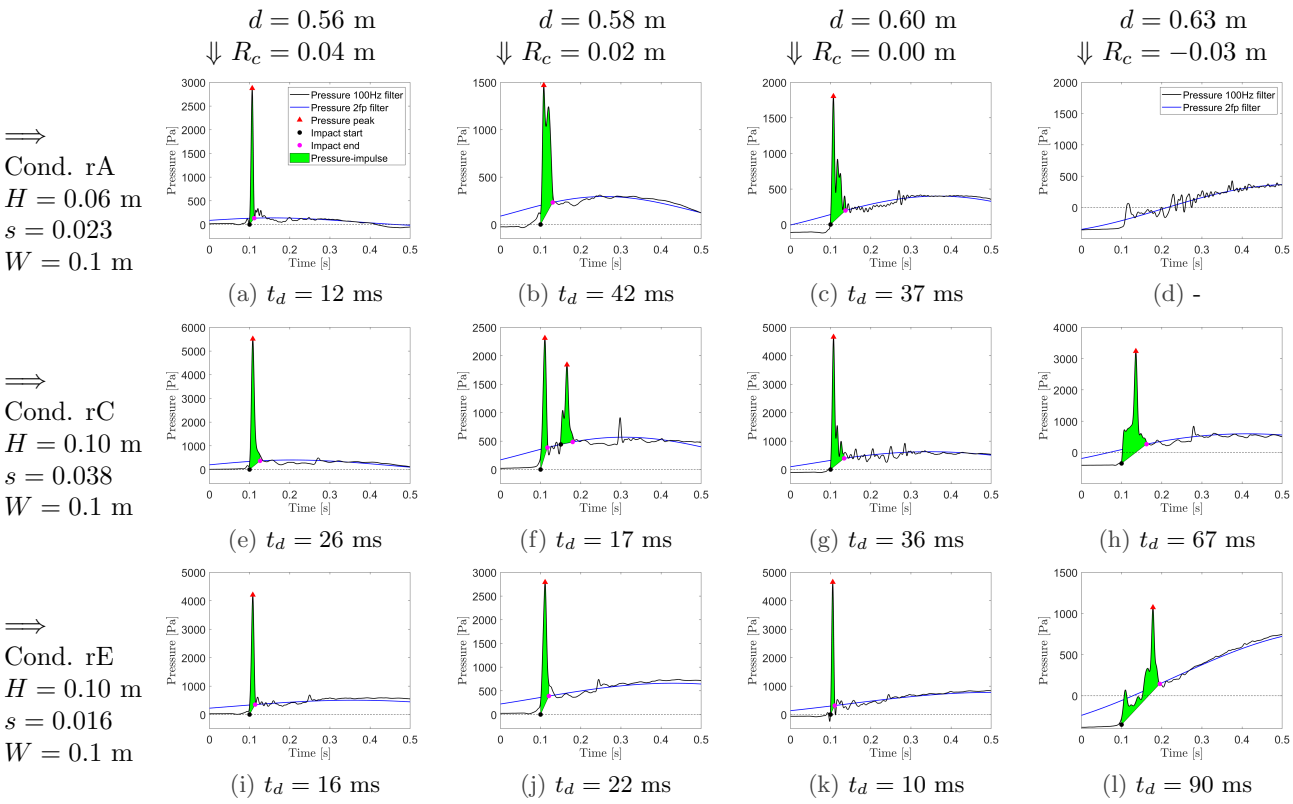

Figure 5: Shorter overhang ($W = 0.1$ m) - Impact types for regular wave tests.

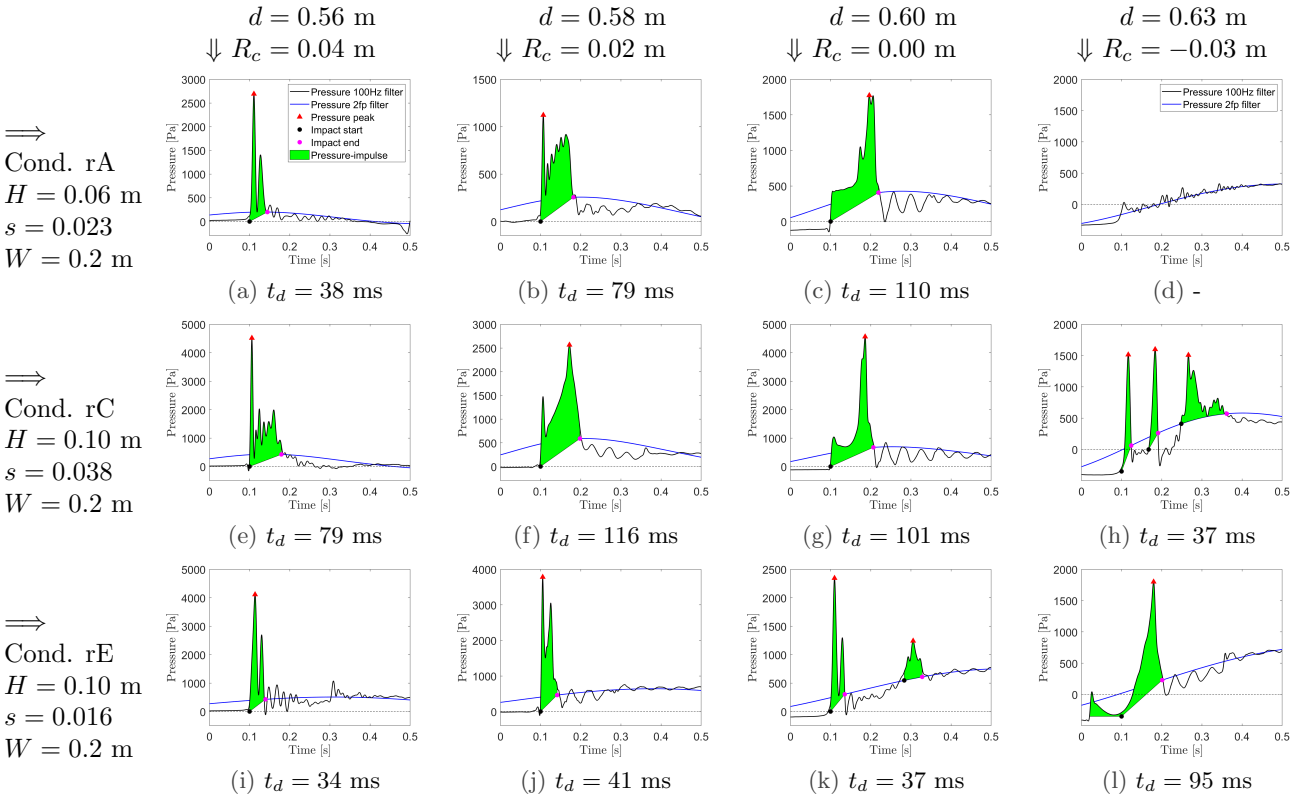

Figure 6: Longer overhang ($W = 0.2$ m) - Impact types for regular wave tests.

bounce-back factor was $\beta = 1.19$ ($\sigma_\beta = 0.15$). This deviates slightly from the values obtained in de Almeida and Hofland (2020*a*) ($\beta = 1.17$ ($\sigma_\beta = 0.11$). The test with a remarkably large dimensionless impulse found in Figure 7 ($\bar{h} = 6$ and $\bar{I} = 2.61$) is showed in Figure 5h corresponding to a condition of negative freeboard, with a very high and long impact. The discussion on the effective bounce-back factor β and its applicability for preliminary load predictions continues in this study in Section 4.3, when the irregular wave tests are considered.

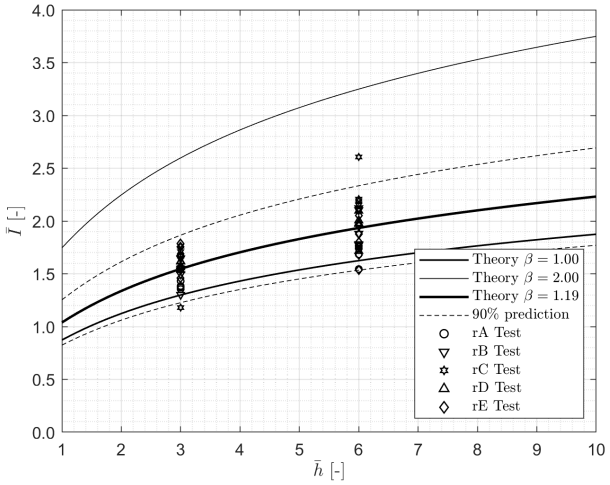

Figure 7: Dimensionless experimental results from regular wave tests with standard configuration.

Spatial variation over the width with standard configuration

The spatial distribution of pressures over the width of the structure was studied in the standard configuration tests. During 10 regular wave tests with standard configuration (5 with shorter overhang and 5 with longer overhang), 7 pressure sensors were placed at the top of the vertical wall along the structure width (see Figure 4c). At this location the wave impact and the highest pressures take place. In addition, an ensemble averaged pressure time series (noted by $\langle\ \rangle$) was calculated as the average pressures from the 7 individual pressure sensors.

Figure 8 summarizes the spatial distribution of pressures over the width for tests without a lateral constriction. The two figures on the left show peak pressures, the two figures on the right show pressure-impulses. Furthermore, the two figures on the top compare individual pressure sensor recordings to the ensemble averaged pressure time series, while the two figures on the bottom show the cross flume distribution. In Figure 8, note that the y-axis scales differ. Figure 8a describes the relation between the pressure peaks measured at the individual pressure sensors with the pressure peaks measured at the ensemble averaged time series. Thus, it is observed that the peak pressures measured by the individual pressure sensors are not observed simultaneously along the whole structure. This leads to a corresponding overestimation of peak forces at the structure if the peak pressure at one location is assumed to take place over the whole width. Figure 8b shows the same comparison for pressure-impulses, and a significantly smaller variability is observed. Based on these observations, it is found that the pressure-impulse measured at one location can be assumed to take place over the whole structure width with a high degree of confidence, while the same cannot be done for pressure peaks. Nevertheless, the spatial distribution of loads obtained in this study may not be directly assumed to take place in other wave impact situations. Still, these results highlight the importance of studying in more detail the spatial distribution of loads during the design of hydraulic structures subjected to wave impacts. The larger variability in the p and P in Figures 8a and 8b (e.g. rBS test for p and rAL for P) is caused by the larger entrapped air pockets, which break down in smaller bubbles during the wave impact and cause a larger loading variability. The cross flume distribution of peak pressures and pressure-impulses are presented in Figure 8c and Figure 8d. Those figures include also a second order polynomial fit for the shorter overhang (blue line), for the longer overhang (red line) and for all tests combined (black line). Figure 8c shows that, besides a variability between the different tests, larger pressure peaks were measured at the sides compared with the centre. Figure 8d shows the same comparison for pressure-impulses, with a similar behaviour but significantly smaller variability.

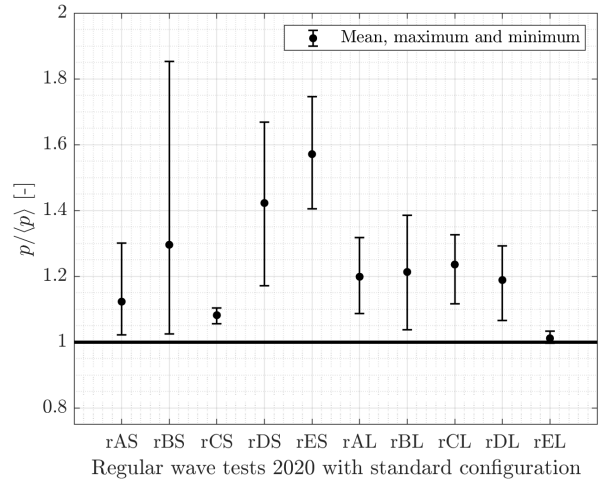

(a) Pressure peak distribution by test

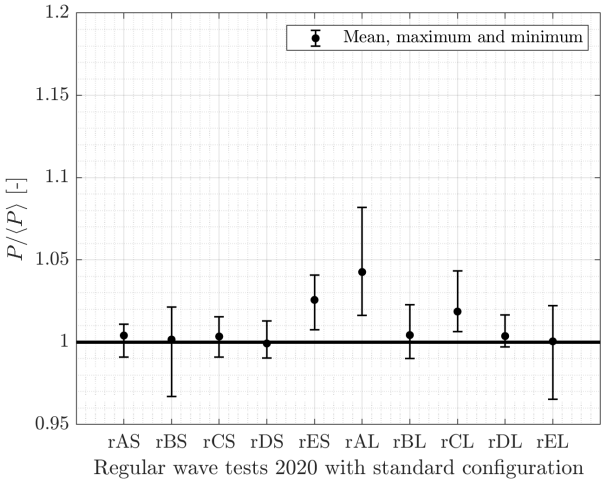

(b) Pressure-impulse distribution by test

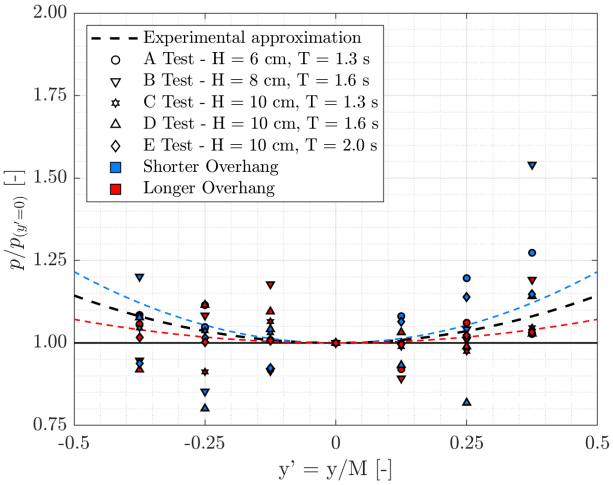

(c) Cross-flume pressure peak distribution

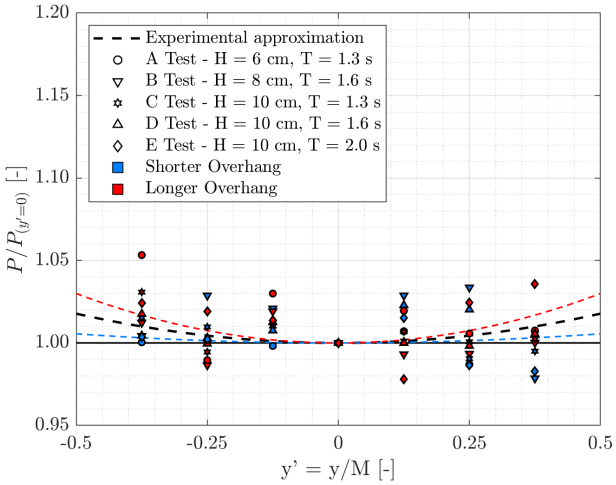

(d) Cross-flume pressure-impulse distribution

Figure 8: Spatial distribution of pressures peaks and pressure-impulses. Note that axis scales differ.

4.2 Regular wave tests with lateral constriction and ventilation gaps

Flood gates often consist of a series of gates that are bordered by pylons or similar lateral constrictions (e.g. Eastern Scheldt, Afsluitdijk, Haringvliet, Fudai or Pont-vannes du Millac). Consequently, those lateral constrictions represent an additional and often-occurring complication in the design of such flood gates. Also, ventilation gaps are present in front of vertical flood gates (e.g. Afsluitdijk), leading to the reduction of wave impact loads. Thus, these two variations of the standard configurations are studied in this section, given their importance for the design of such flood gates. Furthermore, these results also aim to highlight the applicability of the proposed loading prediction expressions to more realistic structural configurations.

Spatial variation over the width with lateral constriction

This section presents the tests with a lateral constriction of 22% of the structure width M. This resembles the presence of a support wall in a flood gate complex as shown in Figure 9. During the 10 tests with a lateral constriction (5 with shorter overhang and 5 with longer overhang), 6 pressure sensors were placed at the top of the vertical wall along the remaining structure width (see Figure 4d). These tests had the goal of studying the spatial distribution of wave impact loadings affected by such three-dimensional structural features.

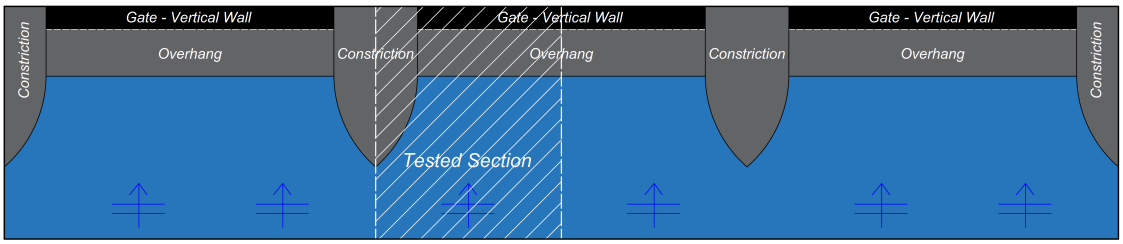

Figure 9: Top view of a schematic flood gate complex with constriction elements.

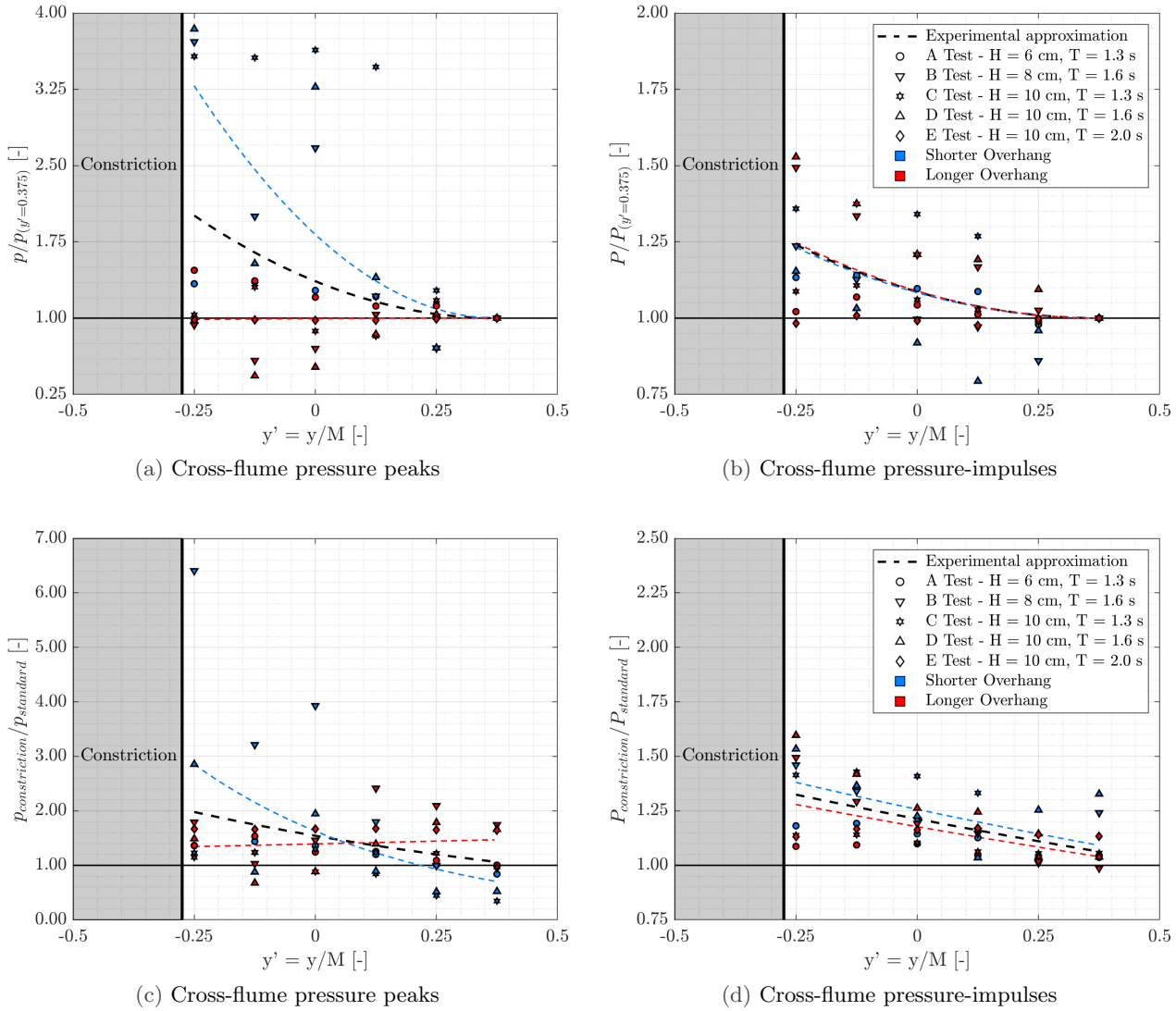

(a) Cross-flume pressure peaks

(b) Cross-flume pressure-impulses

(c) Cross-flume pressure peaks

(d) Cross-flume pressure-impulses

Figure 10: Constriction effect on the spatial distribution of pressures peaks and pressure-impulses.

The results of the tests with a lateral constriction are summarized in Figure 10. The two figures on the left show peak pressures, the two figures on the right show pressure-impulses. Furthermore, the two figures on the top compare individual pressure sensor measurements to the ones at $y' = 0.375$, while the two figures on the bottom compare the results from the tests with a constriction to the tests without a constriction (i.e. the regular wave tests with a standard configuration). All four figures include a second order polynomial fit for the shorter overhang (blue line), for the longer overhang (red line) and for all tests combined (black line). The fit in Figure 10a shows that pressure peaks for the shorter overhang are significantly amplified at the constriction edge. On the contrary, the pressure peaks for the longer overhang remain uniform across the structure. The fit

in Figure 10b shows a clear pattern of amplified pressure-impulses at the constriction edge for both the shorter and the longer overhang. Figure 10c shows that for the shorter overhang the presence of a constriction leads to a large amplification of the pressure peaks at the constriction edge. On the contrary, for the longer overhang, the presence of a constriction leads to a uniform amplification of the pressure peaks along the width of the structure. Figure 10d shows a clear pattern of amplified pressure-impulses at the constriction edge caused by the presence of a constriction for both the shorter and the longer overhang. In summary, the presence of a lateral constriction modifies significantly the spatial distribution of wave loads, amplifying the pressure peaks and pressure-impulses closer to the constriction edge. Besides, the pressure-impulse results show less variability and more predictability compared with the pressure peaks.

Load reducing ventilation gaps

This section describes the effect of ventilation gaps in the reduction of wave impact loads. Figure 11 describes the detailed geometry of the ventilation gaps tested in this study. For the shorter overhang, tests with $G = 1$ cm were carried out, while for the longer overhang, tests with $G = 1$ cm and $G = 2$ cm were carried out. In all tests tests $B = 1$ cm, $B' = 48$ cm and $G' = W - 1$ cm. These ventilation gap dimensions are constant along the whole structure width (i.e $M = 80$ cm). The 30 tests in this experimental set included, besides the three different ventilation gap variations, two different water levels and five different incident wave conditions. This study aims to assess the use of ventilation gaps to reduce wave impact loadings. Thus, the wave impact loads measured in the tests with ventilation gaps are compared to the identical tests (i.e. regular wave tests with standard configuration) carried out in the same test campaign.

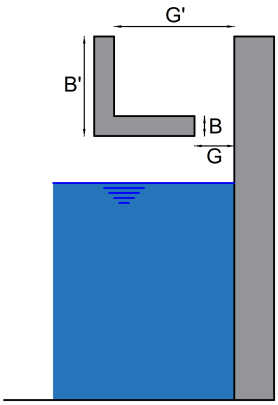

Figure 11: Ventilation gap configuration parameters: inner ventilation gap width G; outer ventilation gap width G'; inner vertical gap boundary B; outer vertical gap boundary B'.

Figure 12 presents all the results for the tests with ventilation gaps, describing the load reduction induced by the presence of a ventilation gap. Figure 12a shows force peaks, while Figure 12b shows force-impulses. In these figures, the test names that include a "58" refer to tests carried at $d = 0.58$ m, while the test names that include a "60" refer to tests carried at $d = 0.60$ m. Figure 12a shows that for the shorter overhang (blue markers), in all cases the presence of a ventilation gap reduced the force peaks. In contrast, for the tests with longer overhangs (red markers), the force peaks in some cases increased with the presence of a ventilation gap. This is explained by the fact that, in those cases, the tests without a ventilation gap lead to very long and low force curves related to the presence of large air entrapments. Thus, in those cases, the presence of a ventilation gap leads to shorter and higher force curves related to the removal of entrapped air. Figures 12b show that in all tests carried out for the shorter and the longer overhangs, the force-impulses were smaller in the tests with ventilation gaps. In summary, the results obtained in this study show that ventilation gaps are effective in reducing standing wave impact loads.

4.3 Irregular wave tests

Up to now, this study presented the analysis of regular waves but, in reality, hydraulic structures are loaded by irregular wave fields. Hence, this section describes the results from the irregular wave tests. The 52 irregular wave tests were carried out for four water levels, five incident wave conditions and two overhang lengths.

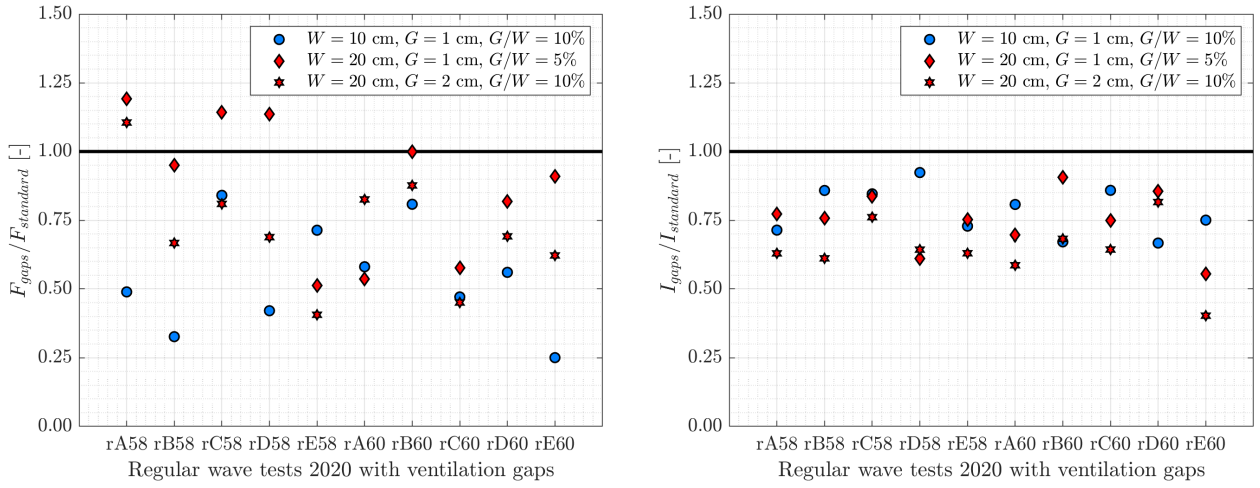

(a) Force peak reduction by test

(b) Force-impulse reduction by test

Figure 12: Effect of ventilation gaps in force peaks and force-impulses.

Furthermore, 50 tests were carried out with 1000 waves, while two extra long tests were carried out with 5000 waves. The spectral incident wave parameters (H_{m0}, T_p) and the incident and reflected wave time series were calculated by the method of Zelt and Skjelbreia (1992) with an array of three wave gauges (see Section 3.3). The time-domain incident wave parameters ($H_{1/3}$, T_m) were obtained from the incident wave time series employing a zero-downcrossing analysis. Further on in this study, the time-domain incident wave parameters are used, instead of the spectral incident wave parameters. For each incident wave propagating towards the structure identified in the zero-downcrossing analysis, the corresponding wave load acting on the structure was identified from the synchronized pressure measurements. For each of these wave loads acting on the structure, the pressure/force peaks and the pressure/force-impulses were obtained in an automatic way for each test.

Figure 13 and Figure 14 summarize the results from all the 52 irregular wave tests. Figure 13 presents the exceedance probability plots for the total force-impulse I (Figure 13a) and for the total force peak F (Figure 13b). Figure 14 illustrates the the relations between force-impulses (I), force peaks (F) and impact durations (t_d). In these figures, a clear difference is observed between force-impulses and force peaks but also between the tests with shorter overhangs and the tests with longer overhangs. The largest force peaks correspond to the smallest impact durations (see Figure 14a), as is also seen for breaking wave impacts (Cuomo et al., 2010). Differently, the largest force-impulses correspond to middle-low impact durations of 30-100 ms (see Figure 14b), in line with the results from Chen et al. (2019). Furthermore, Figures 14a and 14b show that the tests with the longer overhang lead to longer impact durations compared with the tests with shorter overhangs. As discussed in the previous sections, this can be explained by the fact that a longer overhang is directly related to larger air entrapments and thus directly related to longer impact durations (Ramkema, 1978; de Almeida and Hofland, 2020*b*). Furthermore, it is observed that force peaks for both shorter and longer overhangs present similar high values, while significantly higher force-impulses have been measured in the tests with longer overhangs compared with the tests with shorter overhangs. All these conclusions can also be observed in Figure 14c. This figure shows that for equal force peaks, larger force-impulses are measured in the tests with longer overhangs (corresponding to longer impact durations) compared with the tests with shorter overhangs. Also, the extra long tests (5000 waves) present very similar results compared with the standard tests with 1000 waves.

Figure 15 shows the wave impact time series corresponding to the largest force-impulse in each test for the experiments carried out with $R_c = 0$. This condition of zero freeboard corresponds to the largest wave impact velocities at the moment of the wave impact and consequently the largest wave impact loads. Figure 15 shows the diversity of impact magnitudes and characteristics among the different irregular wave test conditions. It can be seen that the irregular wave tests show a less distinct difference between the loading time series of shorter and longer overhangs, as was observed during the regular wave tests (Figures 5 and 6). For example, individual longer impact durations can be found in tests with shorter overhangs (Figure 15c) and individual shorter impact durations can be found in tests with longer overhangs (Figure 15j). Thus, this shows that the dynamic interactions of the incident waves with the structural configurations are even more dynamic and variable in tests with irregular wave conditions.

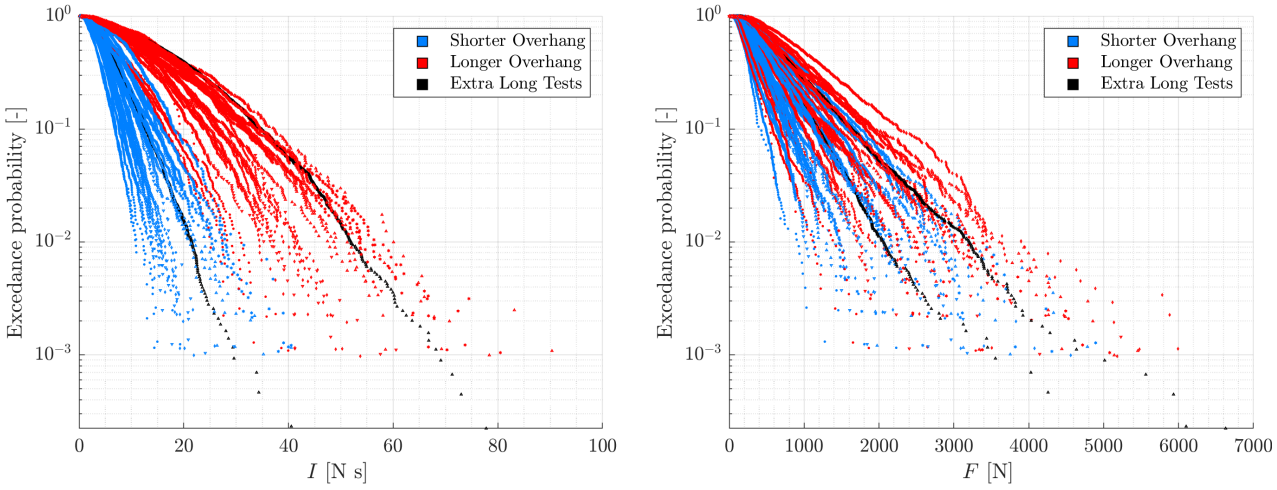

(a) Exceedance force-impulses I (b) Exceedance force peaks F

Figure 13: Exceedance probability per wave impact for force-impulses and force peaks.

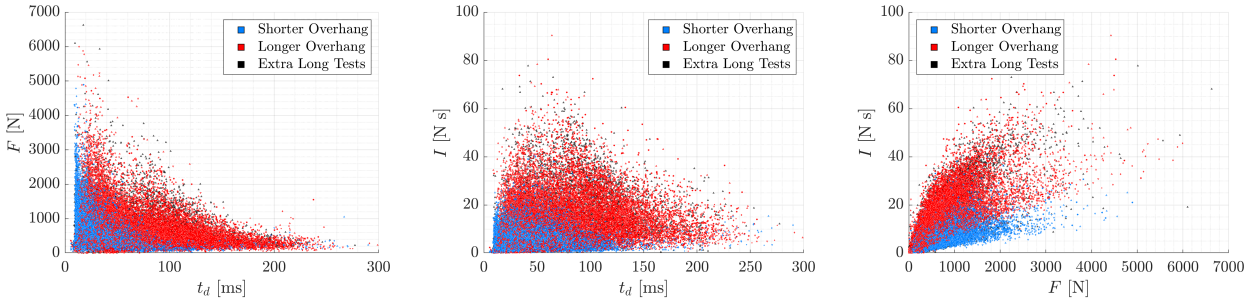

(a) F vs t_d (b) I vs t_d (c) I vs F

Figure 14: Impact duration in relation to force-impulse and force peaks.

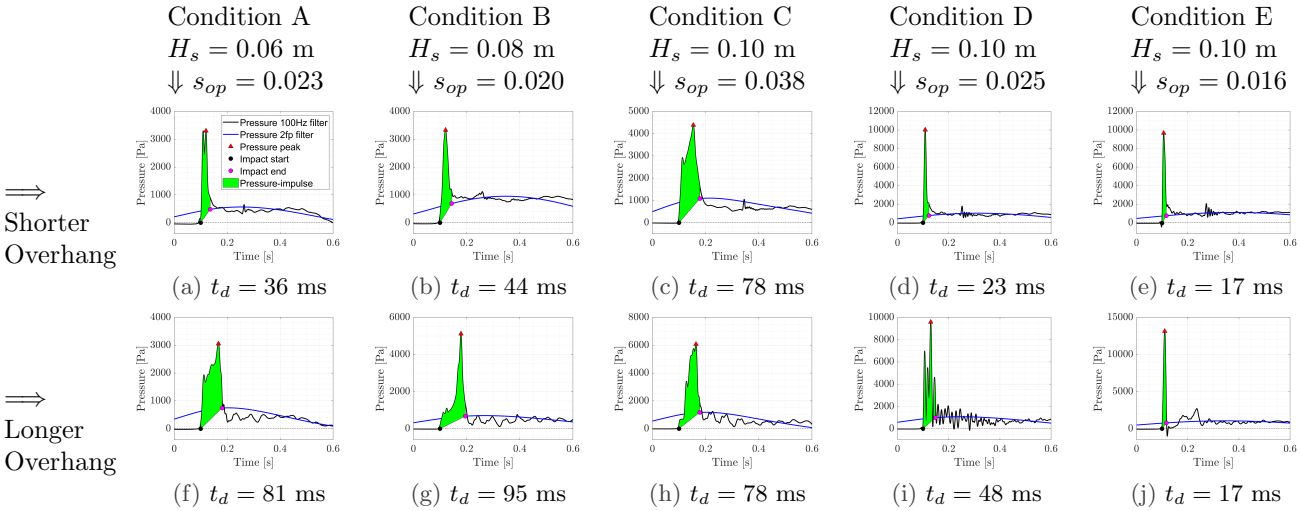

(a) $t_d = 36$ ms (b) $t_d = 44$ ms (c) $t_d = 78$ ms (d) $t_d = 23$ ms (e) $t_d = 17$ ms

(f) $t_d = 81$ ms (g) $t_d = 95$ ms (h) $t_d = 78$ ms (i) $t_d = 48$ ms (j) $t_d = 17$ ms

Figure 15: Wave impact with the maximum force-impulse I for each irregular wave test with $R_c = 0$ m.

To carry out load estimations, it is necessary to predict the effective bounce-back factor β based on wave and structure parameters. To that end, the Gamma Parameter ($\Gamma = U^2 L / gW^2$) is introduced to describe the effective air entrapment characteristics. Figure 16 shows the relation between β and Γ for all irregular and regular wave tests. The Gamma Parameter Γ includes the effect of the wave impact velocity U (i.e. for a larger impact velocity the air has less time to flow away from below the overhang and can be more easily entrapped), and the relation between wave length L and overhang length W (i.e. for a larger relative wave length a more

uniform wave surface can impact parallel to the whole overhang length creating a longer air entrapment). In the irregular waves tests, β was obtained from $I_{1\%}$. More precisely, $I_{1\%}$ is the force-impulse exceeded by 1% of the incident waves. Furthermore, $\bar{I}_{1\%}$ was calculated according to Equation 3, being $U_{1\%}$ the impact velocity determined according to Equation 8 with wave period T_m and wave height $H_{1\%}$ (obtained from Equation 9). This leads to β being calculated as $\beta = \bar{I}_{1\%}/C_I$. Also, for calculating Γ from the irregular wave tests $U_{1\%}$ and L_m were used. This figure shows an upper limit of β around 2, which does not grow further for larger values of Γ. This upper limit of β around 2 is also in agreement with the theoretical limit predicted by Wood et al. (2000), in which $(1 < \beta < 2)$. Figure 16 also shows the range of data collected in this study, showing that regular wave tests had lower values of Γ compared to the irregular wave tests. For this reason, the experimental approximation shown in the figure ($R^2 = 0.83$, $RMSE = 0.12$) only includes the irregular wave tests, although the regular wave test results are also in agreement. An outlier value of $\beta = 0.63$ from the irregular wave tests can be seen and is not included in the approximation. It corresponds to the test with the longer overhang ($W = 0.2$ m), the smallest incident wave condition (Condition A) and the highest water level with a negative freeboard ($d = 0.63$ m, $R_c = -0.03$ m). In this condition the incident waves were not able to reach and impact the overhang at the vertical wall, leading to this low value of β. This is in line with the results from the regular wave tests, in which the smallest incident waves did not produce wave impacts for the tests with the highest water level with a negative freeboard ($d = 0.63$ m, $R_c = -0.03$ m), see Figures 5d and 6d. In summary, Figure 16 and Equation 10 can be used for calculating effective bounce-back factor β using the Gamma Parameter Γ for carrying out loading estimations, as it will be introduced hereafter.

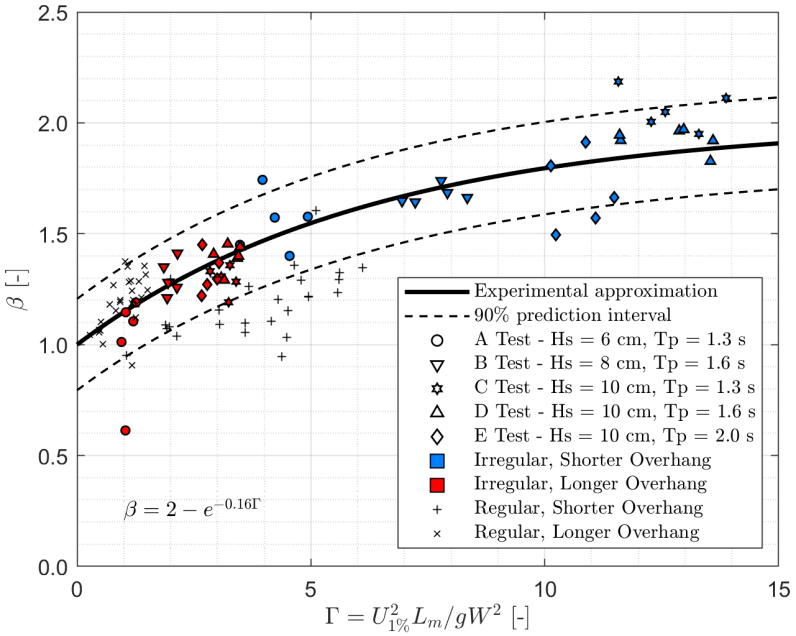

Figure 16: Summary of experimental laboratory results for the effective bounce-back factor

$$\beta = 2 - e^{-0.16\Gamma} \tag{10}$$

Figure 17 compares the measured force-impulses in irregular wave tests (markers), with the loading predictions (lines). The loading predictions in this figure were calculated using Figure 16 and Equation 10 for obtaining β, Equation 9 (for obtaining H), Equation 8 (for obtaining U), Equation 4 (for obtaining $\bar{I}$) and Equation 3 (for obtaining I). In Figure 17, the figures on the top row show the tests with the shorter overhang, while the figures in the bottom row show the tests with the longer overhang. Furthermore, the two figures on the left show the comparison for $R_c = 0.04$ m, while the two figures on the right show the comparison for $R_c = 0.00$ m. The results shown in Figure 17 illustrates that the loading prediction expressions presented in this study can be used for preliminary loading estimations for standing wave impacts on relatively short overhangs. The largest deviations between the measured and predicted loads are found for the most energetic wave conditions, and is considered to be closely related to the variations in the air entrapment dimensions. Following these results, the previously described loading prediction expressions are found to be sufficiently accurate for a variety of incident wave characteristics, standard and extra long tests, different overhang lengths and different water levels.

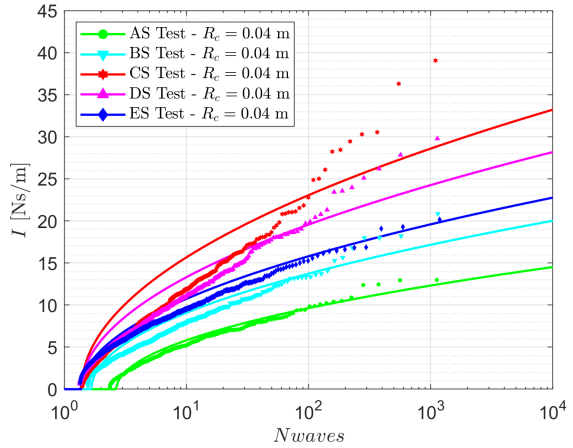

(a) Shorter overhang, $R_c = 0.04$ m

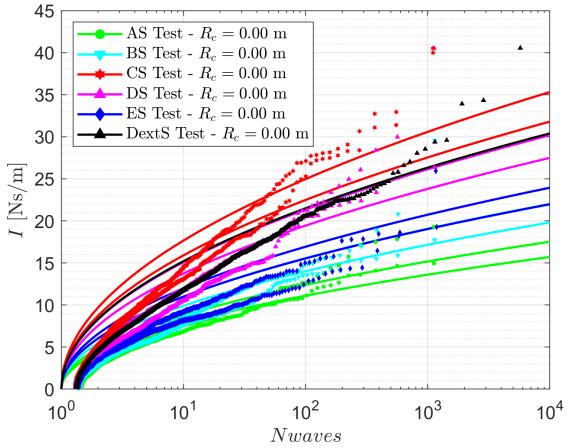

(b) Shorter overhang, $R_c = 0.00$ m

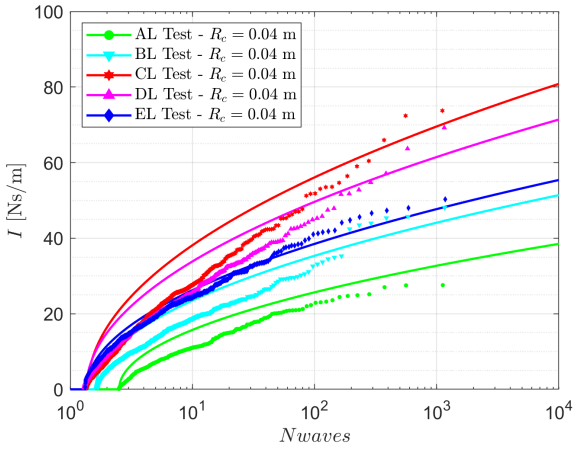

(c) Longer overhang, $R_c = 0.04$ m

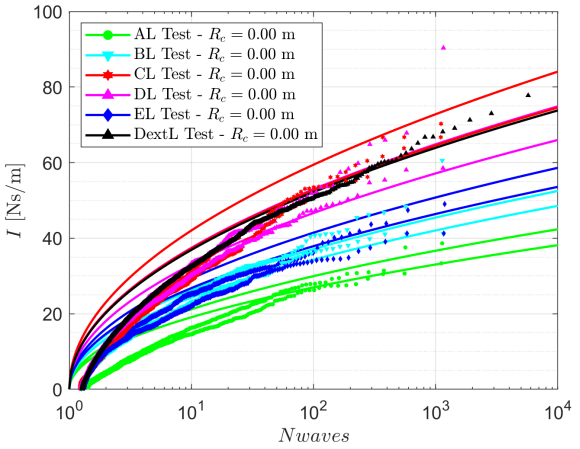

(d) Longer overhang, $R_c = 0.00$ m

Figure 17: Predicted (lines) and measured (markers) force-impulse exceedance curves per incident wave.

5 Discussion

This section discusses the results from this study, including the regular wave tests with the standard configuration, the spatial distribution of wave impact loads over the structure width, the effect of load reducing ventilation gaps and the irregular wave tests.

From the regular wave tests with standard configuration, a large number of findings were presented in Section 4.1. Furthermore, extended validation of the pressure impulse theory was found (see Figure 7). Nevertheless, the relatively constant effective bounce-back factors β from the regular wave tests were not directly confirmed by the irregular wave tests. This is explained by the fact that the regular wave tests consisted of significantly less extreme wave impacts (i.e. lower Γ) compared with the irregular wave results (see Figure 16). Thus, two conclusions can be drawn regarding the regular wave test results. First, that the results of regular waves alone were not sufficient for describing loading prediction expressions for preliminary design. To this end, irregular wave tests were used, as addressed in Section 4.3. Second, besides the previously mentioned aspects, the extended validation this study presents based on regular and irregular waves offer sufficient confidence that the pressure-impulse theory can be used for describing the impulsive loading generated by standing wave impacts.

Two remarks may be added regarding the pressure measurements shown in Figures 5 and 6. First, vibrations on the pressure measurements are observed in many tests, mainly in the tests with longer overhangs (see Figures 6a, 6b, 6e, 6i and 6j), but also in the tests with shorter overhangs (see Figures 5c and 5g). These vibrations took place mainly during the wave impacts but also after the wave impacts. All pressure vibrations recorded during the wave impacts showed a different vibration frequency. This indicates that these vibrations are related to the

dimensions of the entrapped air, which varies between the different tests and to a smaller extend between every single wave impact. The post-impact vibrations also showed the same pattern, of unique vibrations frequencies in each test, besides one exception for the longest wave impacts found in the tests with the longer overhang. For the longest wave impacts with the longer overhang, with impact durations larger than 100 ms (see Figures 6c, 6f and 6g), a vibration pattern of 22 Hz is visible after the wave impacts. This vibration pattern originates in the flume bottom, which responds in a dynamic way to the longest impact durations. This illustrates the importance of considering the dynamic response of all elements of the test setup in wave impact laboratory experiments. Second, in the tests with $R_c \leq 0$ m, (e.g. Figures 5c and 6c) the pressure recording is below zero before the wave impact, while in the tests with $R_c > 0$ m, (e.g. Figures 5a, and 6a) the pressure recording is approximately at zero before the wave impact. In the tests with $R_c > 0$ m, the pressure sensor is in contact with the air at the start of the test, the same condition as before the wave impact. On the contrary, in the tests with $R_c \leq 0$ m the pressure sensor is in contact with water at the start of the test, while before the wave impact the pressure sensor is in contact with air. This deviation from zero in the tests with $R_c \leq 0$ includes the hydrostatic pressure difference for the pressure sensor measurements at $z = 0.59$ m shown in Figures 5 and 6. The temperature effect of the pressure sensors is found to be reduced in the case of the Kulite HKM-375M-SG and do not influence any conclusion from this study. Nevertheless, the performance of the instrumentation used in wave impact studies (e.g. the temperature effect of pressure sensors), should always be examined.

In the tests with a lateral constriction, a particular load pattern was found for test rES (test condition rE with the shorter overhang) caused by a cross-flume wave resonance pattern. This can be observed in Figure 18 (where all 10 constriction test results are included) in comparison with Figure 10 (where only 9 constriction test results are included, excluding the mentioned rES condition). Note that the y-axis scales differ between the two figures (i.e. Figure 10 and Figure 18). This cross-flume wave resonance pattern was not only observed in the analysis of the test results but also clearly visible during the laboratory tests. This wave resonance pattern is not expected to take place in an irregular wave field because the frequency of the irregular incident waves is not constant. Thus, this test condition was not considered in the analysis of the spatial distribution over the width presented earlier in this study in Section 4.2.

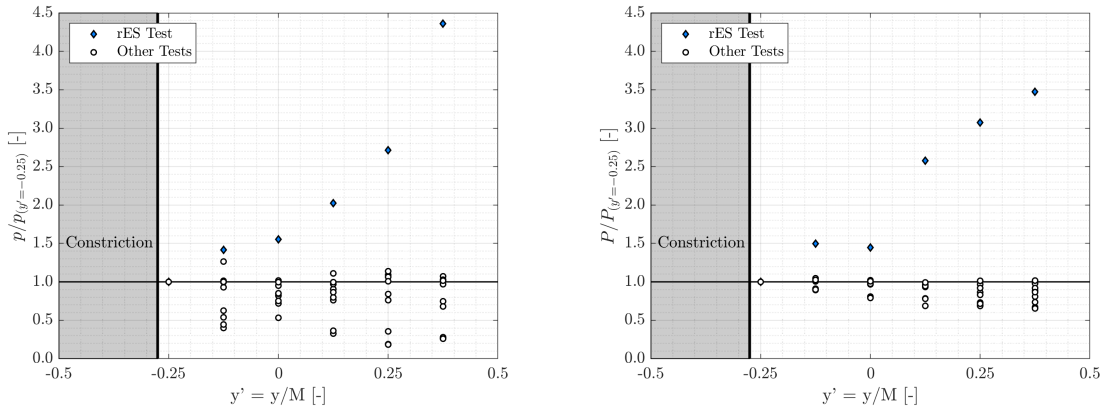

(a) Cross-flume pressure peaks

(b) Cross-flume pressure-impulses

Figure 18: Constriction effect on the spatial distribution of pressures peaks and pressure-impulses.

In the experiments with load reducing ventilation gaps, two ventilation gap widths were tested (i.e. $G = 1$ cm and $G = 2$ cm, see Section 4.2 and Figure 11). In addition, the other ventilation gap dimensions were constant in all tests (i.e. $B = 1$ cm, $B' = 48$ cm and $G' = W - 1$ cm). Thus, these geometric characteristics should be taken into account when assessing the effect of load reducing ventilation gaps. Other configurations, such as the ones presented in Figure 19 (i.e. with equal G but with variations in G', B or B') may lead to different results regarding the effect of ventilation gaps for reducing standing wave impact loads. In summary, for assessing the effect of loading ventilation gaps, the precise configuration of such gaps should be described with sufficient precision (i.e. not only the inner ventilation gap width G) in order to have a higher degree of confidence in the corresponding load reduction.

In the irregular wave tests, the effective bounce-back factor β was calculated from $I_{1\%}$. This exceedance level was used for describing the effective bounce-back factor β for extreme wave impacts given its expected reduced statistical variation, and it allowed the derivation of preliminary load prediction expressions. In addition, this

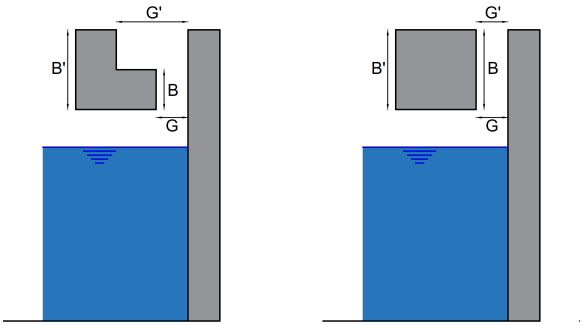

(a) (b)

Figure 19: Alternative ventilation gaps configurations.

study carried out 50 tests of 1000 waves, and two tests of 5000 waves. Nevertheless, for a more complete definition of the extreme distribution of wave impact loads, additional longer tests may be considered. This would provide a better description of the wave impact magnitudes with a very small exceedance probability. Also, this study includes laboratory experiments with a reduced scale, from which the loading prediction expressions are calibrated (i.e. β). Thus, the study on the scaling of such loading prediction expressions to prototype structures should be considered. This should include in particular the effect and scaling of entrapped air, following the work from Mitsuyasu (1966) and Ramkema (1978). Furthermore, in the load prediction expressions described in Section 4.3 the mean wave period T_m is used. Figure 20 discusses this assumption based on experimental results. Figure 20a presents the results for the tests with shorter overhangs, while Figure 20b presents the results for the tests with longer overhangs. These two figures show that for the largest wave impact velocities in each test, a relation of T/T_m close to 1 is observed. Further, the distribution of wave periods T and its relation with T_m were in agreement with Goda (2010). Based on these observations, it is concluded that the use of the mean wave period T_m for preliminary load predictions is sufficiently accurate at this stage.

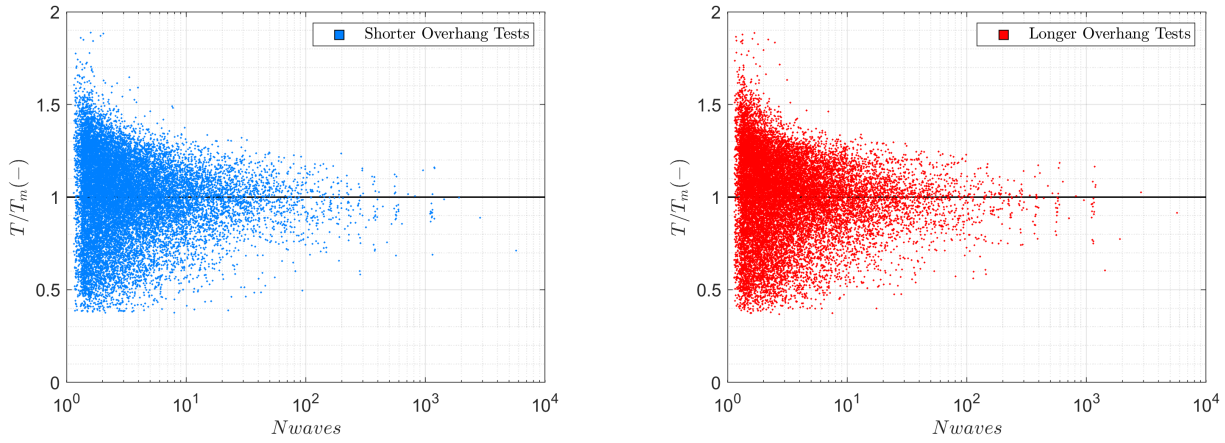

(a) Shorter Overhang (b) Longer Overhang

Figure 20: Return period of U vs T/T_m.

6 Conclusions

This section summarizes the main conclusions on wave loading on vertical structures in consequence of standing wave impacts on an adjacent relatively short overhang, with an emphasis on describing this loading using the pressure-impulse theory. This paper addressed two complementary objectives. Firstly, it extends the knowledge on standing wave impacts addressing the following aspects: changes in hydraulic loading conditions (regular/irregular waves and varying freeboards) and changes in the structure geometry (lateral constriction and loading reducing ventilation gaps). Secondly, it presents loading prediction expressions for preliminary loading estimations built up by the previously developed pressure-impulse theory that is empirically calibrated using the presently acquired experimental data.

The standard regular wave tests describe the influence of the overhang length, incident conditions and water levels on the wave impact loading characteristics and magnitudes, including the spatial distribution. First, the tests with the shorter overhangs presented shorter, higher and less variable wave impact loading signals compared to the tests with longer overhangs. Second, the different incident wave conditions lead to different loading characteristics and magnitudes. Identical loading behaviour was found for repeated tests with equal incident wave conditions. Third, the change in water levels affected the wave impact loading magnitudes as predicted, with higher loads measured in tests with smaller freeboards. On tests with the water level higher than the overhang level (i.e. negative freeboard), a significantly more variable behaviour was observed. Also, during the tests with the shorter overhang, lower water levels were strongly related to shorter impact durations. In the tests with the longer overhang, lower water levels were only partially related to shorter impact durations. Fourth, it was found that the pressure peaks measured at one location does not take place instantly along the whole structure width. Thus, pressure peaks at one single location were found to be higher than the pressure peaks of the averaged pressure signal. On the contrary, the pressure-impulse at one single location was found to be very similar to the pressure-impulses of the averaged pressure signal.

The constriction tests showed the effect of such a lateral constriction on the spatial distribution of the wave impact loading. The presence of a lateral constriction modifies significantly the spatial distribution of wave loads, amplifying the pressure peaks and pressure-impulses closer to the constriction edge. The ventilation gap tests showed the effect of such ventilation gaps on the reduction of wave impact loadings. First, force peaks were lower in most of the tests with the presence of a ventilation gap, in comparison to tests without ventilation gaps. An increase in force peaks was only found in some tests with longer overhangs, explained by the fact that without a ventilation gap these tests showed long and lower force curves related to the presence of larger air entrapments. Thus, in those cases, the presence of a ventilation gap leads to shorter and higher force curves related to the removal of entrapped air. Second, force-impulses were always lower for all test conditions with the presence of a ventilation gap, in comparison to tests without ventilation gaps. This data highlights thus the effect of ventilation gaps on reducing wave impact loadings.

The irregular wave tests contributed to extending previous conclusions towards design applications. This study includes both standard and extra long irregular wave tests, from which a few remarks should be made. First, and differently from regular wave tests, irregular wave tests showed a large range of different loading curves in all overhang lengths and water levels. This highlighted that the dynamic interactions of the incident waves with the structural configurations are even more dynamic and variable in irregular wave conditions. Second, the largest force peaks corresponded to the smallest impact durations, while the largest force-impulses corresponded to middle-low impact durations of 30-100 ms. Third, the irregular wave tests allowed to describe loading prediction expressions for preliminary loading estimations. To that end, the Gamma Parameter ($\Gamma = U^2L/gW^2$) is introduced to describe the effective air entrapment characteristics. Furthermore, the relation between the effective bounce-back factor ($1 < \beta < 2$) with the Gamma Parameter Γ was presented ($\beta = 2 - e^{-0.16\Gamma}$). These expressions presented in this study were shown to be suitable for carrying out load estimations for standing wave impacts on vertical hydraulic structures with relatively short overhangs.

This study constitutes a step forward in the study of confined wave impacts. In particular, the load prediction expressions based on the Gamma Parameter Γ overcomes a significant knowledge gap and provide a validated design tool for this type of wave impact. Nevertheless, this study also presents two main limitations to its applicability in design. Firstly, this study includes schematic representations of a vertical hydraulic structure with relatively short overhangs in a flat bottom subjected only to normally incident waves. Thus, for its use in design, the conclusions of this study should be combined with the detailed analysis of the structure geometry, the incident wave characteristics and the local bathymetry particularities. Secondly, this study is based on laboratory experiments with a reduced scale. Thus, for its use in design, the scaling of loads and wave impact processes (e.g. air entrapment and impact duration) should be considered. Additional research on standing wave impacts on vertical hydraulic structures with overhangs may continue in the future and may include experimental, analytical and numerical methods. This would allow to further reduce the uncertainties and increase the reliability in the design of vertical hydraulic structures with overhangs. This is particularly relevant for thin steel structures such as flood gates which are especially susceptible to a dynamic behaviour under such impulsive wave impact loads.

Notations

Name	Symbol	Unit
Total wave amplitude at wall	A_w	m
Inner vertical gap boundary	B	m
Outer vertical gap boundary	B'	m
Theoretical dimensionless force-impulse	C_I	-
Wave reflection coefficient	c_r	-
Still water depth	d	m
Force	F	N
Gravitational acceleration	g	m/s^2
Inner ventilation gap width	G	m
Outer ventilation gap width	G'	m
Overhang height	h	m
Dimensionless overhang height	$\bar{h}$	-
Wave height	H	m
Time domain significant wave height	$H_{1/3}$	m
Frequency domain significant wave height	H_{m0}	m
Significant wave height	H_s	m
Force-impulse	I	N s
Dimensionless force-impulse	$\bar{I}$	-
Wave length	L	m
Wave length based on T_m	L_m	m
Wave length based on T_p	L_p	m
Deep water wave length	L_0	m
Structure width	M	m
Pressure	p	Pa
Pressure-impulse	P	Pa s
Dimensionless pressure-impulse	$\bar{P}$	-
Exceedance probability	pr	-
R-Square coefficient of determination	R^2	-
Freeboard	R_c	m
Root mean squared error	$RMSE$	-
Wave steepness	s	-
Deep water wave steepness	s_0	-
Wave period	T	s
Mean wave period	T_m	s
Peak wave period	T_p	s
Wave impact duration	t_d	s
Impact velocity	U	m/s
Overhang length	W	m
Dimensionless overhang length	$\bar{W}$	-
Effective bounce-back effect	β	-
Gamma Parameter	Γ	-
Wave surface position	η	m
Wave surface velocity	$\dot{\eta}$	m/s
Peregrine Number	Λ	-
Angular wave frequency	ω	rad/s
Fluid density	ρ	kg/m^3

Acknowledgements

This study is part of the DynaHicS (Dynamics of Hydraulic Structures) Project, supported by NWO (Nederlandse Organisatie voor Wetenschappelijk Onderzoek) grant ALWTW.2016.041. The authors would like to thank Sander de Vree for his support during the experiments carried out at Delft University of Technology.

Author contributions (CRediT)

EdA: conceptualization, methodology, design and execution of laboratory experiments, validation, investigation, software, writing-review and editing, formal analysis, data curation, writing-original draft preparation and visualization. BH: conceptualization, methodology, validation, investigation, software, writing-review and editing, resources, supervision, project administration and funding acquisition.

References

Bagnold, R.A. (1939). Wave-pressure research. *The institution of Civil Engineers*, **12**, 202 – 226.

Bogaert, H. (2018). *An experimental investigation of sloshing impact physics in membrane LNG tanks on foating structures*. Ph.D. thesis, Delft University of Technology,.

Castellino, M., Romano, A., Lara, J.L., Losada, I.J. and De Girolamo, P. (2021). Confined-crest impact: Forces dimensional analysis and extension of the goda's formulae to recurved parapets. *Coastal Engin.*, **163**, 103814.

Castellino, M., Sammarco, P., Romano, A., Martinelli, L., Ruol, P., Franco, L. and Girolamo, P.D. (2018). Large impulsive forces on recurved parapets under non-breaking waves. a numerical study. *Coastal Engin.*, **136**, 1 – 15.

Chen, X., Hofland, B., Altomare, C., Suzuki, T. and Uijttewaal, W. (2015). Forces on a vertical wall on a dike crest due to overtopping flow. *Coastal Engin.*, **95**, 94 – 104.

Chen, X., Hofland, B., Molenaar, W., Capel, A. and van Gent, M. (2019). Use of impulses to determine the reaction force of a hydraulic structure with an overhang due to wave impact. *Coastal Engin.*, **147**, 75 – 88.

Chen, X., Hofland, B. and Uijttewaal, W. (2016). Maximum overtopping forces on a dike-mounted wall with a shallow foreshore. *Coastal Engin.*, **116**, 89 – 102.

Cooker, M.J. and Peregrine, D.H. (1990). A model for breaking wave impact pressures. In: *Proc. Coastal Engin. Conference 1990*. Delft, The Netherlands.

Cooker, M.J. and Peregrine, D.H. (1995). Pressure-impulse theory for liquid impact problems. *Journal of Fluid Mechanics*, **297**, 193 – 214.

Cuomo, G., Allsop, W., Bruce, T. and Pearson, J. (2010). Breaking wave loads at vertical seawalls and breakwaters. *Coastal Engin.*, **57**(4), 424 – 439.

Cuomo, G., Tirindelli, M. and Allsop, W. (2007). Wave-in-deck loads on exposed jetties. *Coastal Engin.*, **54**(9), 657 – 679.

de Almeida, E. and Hofland, B. (2020*a*). Validation of pressure-impulse theory for standing wave impact loading on vertical hydraulic structures with short overhangs. *Coastal Engin.*, **159**, 103702.

de Almeida, E. and Hofland, B. (2020*b*). Experimental observations on impact velocity and entrapped air for standing wave impacts on vertical hydraulic structures with overhangs. *J. Mar. Sci. Eng.*, **8**(11), 857.

Dermentzoglou, D., Castellino, M., De Girolamo, P., Partovi, M., Schreppers, G.J. and Antonini, A. (2021). Crownwall failure analysis through finite element method. *Journal of Marine Science and Engineering*, **9**(1).

Dias, F. and Ghidaglia, J.M. (2018). Slamming: Recent progress in the evaluation of impact pressures. *Annual Review of Fluid Mechanics*, **50**(1), 243–273.

Goda, Y. (1974). A new method of wave pressure calculation for the design of composite breakwater. In: *Proc. Coastal Engin. Conference 1974*. Copenhagen, Denmark.

Goda, Y. (2010). *Random seas and design of maritime structures*. World Scientific, Singapore, 3rd edition.

Hayatdavoodi, M., Seiffert, B. and Ertekin, R.C. (2014). Experiments and computations of solitary-wave forces on a coastal-bridge deck. part ii: Deck with girders. *Coastal Engin.*, **88**, 210 – 228.

Hedges, T. (1995). Regions of validity of analytical wave theories. In: *Proc. ICE Water Maritime and Energy 1995*. London, United Kingdom.

Hofland, B. (2015). Modeltesten golfkrachten spuisluizen afsluitdijk. Meetrapport 1220263, Deltares, Delft, The Netherlands.

Kisacik, D., Troch, P., Bogaert, P.V. and Caspeele, R. (2014). Investigation of uplift impact forces on a vertical wall with an overhanging horizontal cantilever slab. *Coastal Engin.*, **90**, 12 – 22.

Longuet-Higgins, M. (1952). On the statistical distribution of the heights of sea waves. *Journal of Marine Research*, **11**(3), 245 – 266.

Martinelli, L., Ruol, P., Volpato, M., Favaretto, C., Castellino, M., Girolamo, P.D., Franco, L., Romano, A. and Sammarco, P. (2018). Experimental investigation on non-breaking wave forces and overtopping at the recurved parapets of vertical breakwaters. *Coastal Engin.*, **141**, 52 – 67.

McConnell, K., Allsop, W. and Cruickshank, I. (2004). *Piers, jetties and related structures exposed to waves: Guidelines for hydraulic loadings*. Thomas Telford Publishing, London, United Kingdom.

Minikin, R.R. (1950). *Winds, waves and maritime structures*. Griffin, London, United Kingdom.

Mitsuyasu, H. (1966). Shock pressure of breaking wave. In: *Proc. Coastal Engin. Conference 1996*. Orlando, United States.

Oumeraci, H., Kortenhaus, A., Allsop, W., de Groot, M., Crouch, R., Vrijling, H. and Voortman, H. (2001). *Proverbs: Probabilistic design tools for vertical breakwaters*. Balkema, Lisse.

Ramkema, C. (1978). A model law for wave impacts on coastal structures. In: *Proc. Coastal Engin. Conference 1978*. Hamburg, Germany.

Renzi, E., Wei, Y. and Dias, F. (2018). The pressure impulse of wave slamming on an oscillating wave energy converter. *Journal of Fluids and Structures*, **82**, 258 – 271.

Seiffert, B., Hayatdavoodi, M. and Ertekin, R.C. (2014). Experiments and computations of solitary-wave forces on a coastal-bridge deck. part i: Flat plate. *Coastal Engin.*, **88**, 194 – 209.

Sonneville, B., Hofland, B., Mowinckel, A. and Paulsen, B. (2015). Wave impact loads on offshore gravity based structure. In: *Proc. OMAE Conference 2015*. St. John's, Canada.

Takahashi, S., Tanimoto, K. and Shimosako, K. (1994). A proposal of impulsive pressure coefficient for design of composite breakwaters. In: *Proc. International Conference of Hydro-Technical Engineering for Port and Harbour Construction 1994*. Yokosuka, Japan.

Tieleman, O., Hofland, B., Tsouvalas, A., de Almeida, E. and Jonkman, S. (2021). A fluid–structure interaction model for assessing the safety of flood gate vibrations due to wave impacts. *Coastal Engineering*, **170**, 104007.

Tieleman, O.C., Tsouvalas, A., Hofland, B. and Jonkman, S.N. (2019). A three dimensional semi-analytical model for the prediction of gate vibrations. *Marine Structures*, **65**, 134 – 153.

WL (1977). Wave impacts on the gate in the eastern scheldt caisson (in dutch: Golfklappen op de schuif in de oosterschelde-caisson). Verslag M 1335 deel I, WL Delft Hydraulics (presently Deltares), Delft, The Netherlands.

WL (1978). Wave impacts against concrete perforated gates (in dutch: Golfklappen tegen betonnen roosterschuiven). Verslag M 1381 deel II, WL Delft Hydraulics (presently Deltares), Delft, The Netherlands.

WL (1979). Wave impacts: A literature review and scale effects in model studies (in dutch: Golfklappen: een literaturroverzicht en schaaleffekten in modelonderzoek). Verslag M 1335 deel III, WL Delft Hydraulics (presently Deltares), Delft, The Netherlands.

Wood, D.J. and Peregrine, D.H. (1996). Wave impact beneath a horizontal surface. In: *Proc. Coastal Engin. Conference 1996*. Orland, United States.

Wood, D.J., Peregrine, D.H. and Bruce, T. (2000). Study of wave impact against a wall with pressure-impulse theory. i: trapped air. *Journal of Waterway, Port, Coastal and Ocean Engineering*, **126**(4), 182 – 190.

Zelt, J. and Skjelbreia, J. (1992). Estimating incident and reflected wave fields using an arbitrary number of wave gauges. In: *Proc. Coastal Engin. Conference 1992*. Venice, Italy.

A Appendix - Tables

Table A1: Summary of the configurations tested for each hydrodynamic condition. Incident wave characteristics shown in this table are the target wave conditions. "x1", "x2", and "x3" repesent the number of repetitions for the $W = 0.1$ m (S) and $W = 0.2$ m (L) overhangs.

Regular Wave Tests - Standard (50 waves/test) and Gaps/Constriction (25 waves/test)																				
d [m]	R_c [m]	Condition rA				Condition rB				Condition rC				Condition rD				Condition rE			
		H	T	L_0	s_0	H	T	L_0	s_0	H	T	L_0	s_0	H	T	L_0	s_0	H	T	L_0	s_0
		0.06 m	1.3 s	2.64 m	0.023	0.08 m	1.6 s	3.99 m	0.020	0.10 m	1.3 s	2.64 m	0.038	0.10 m	1.6 s	3.99 m	0.025	0.10 m	2.0 s	6.24 m	0.016
0.56	0.04	Standard: S (x1) + L (x1)				Standard: S (x1) + L (x1)				Standard: S (x1) + L (x1)				Standard: S (x1) + L (x1)				Standard: S (x1) + L (x1)			
0.58	0.02	Standard: S (x1) + L (x1) Gaps: S (x1) + L (x2)				Standard: S (x1) + L (x1) Gaps: S (x1) + L (x2)				Standard: S (x1) + L (x1) Gaps: S (x1) + L (x2)				Standard: S (x1) + L (x1) Gaps: S (x1) + L (x2)				Standard: S (x1) + L (x1) Gaps: S (x1) + L (x2)			
0.60	0.00	Standard: S (x3) + L (x3) Gaps: S (x1) + L (x2) Constriction: S (x1) + L (x1)				Standard: S (x2) + L (x2) Gaps: S (x1) + L (x2) Constriction: S (x1) + L (x1)				Standard: S (x2) + L (x2) Gaps: S (x1) + L (x2) Constriction: S (x1) + L (x1)				Standard: S (x2) + L (x2) Gaps: S (x1) + L (x2) Constriction: S (x1) + L (x1)				Standard: S (x3) + L (x3) Gaps: S (x1) + L (x2) Constriction: S (x1) + L (x1)			
0.63	-0.03	Standard: S (x1) + L (x1)				Standard: S (x1) + L (x1)				Standard: S (x1) + L (x1)				Standard: S (x1) + L (x1)				Standard: S (x1) + L (x1)			
Irregular Wave Tests - Standard (1000 waves/test) and Extra Long (5000 waves/test)																					
d [m]	R_c [m]	Condition A				Condition B				Condition C				Condition D				Condition E			
		H_s	T_p	L_{0p}	s_{0p}	H_s	T_p	L_{0p}	s_{0p}	H_s	T_p	L_{0p}	s_{0p}	H_s	T_p	L_{0p}	s_{0p}	H_s	T_p	L_{0p}	s_{0p}
		0.06 m	1.3 s	2.64 m	0.023	0.08 m	1.6 s	3.99 m	0.020	0.10 m	1.3 s	2.64 m	0.038	0.10 m	1.6 s	3.99 m	0.025	0.10 m	2.0 s	6.24 m	0.016
0.56	0.04	Standard: S (x1) + L (x1)				Standard: S (x1) + L (x1)				Standard: S (x1) + L (x1)				Standard: S (x1) + L (x1)				Standard: S (x1) + L (x1)			
0.58	0.02	Standard: S (x1) + L (x1)				Standard: S (x1) + L (x1)				Standard: S (x1) + L (x1)				Standard: S (x1) + L (x1)				Standard: S (x1) + L (x1)			
0.60	0.00	Standard: S (x2) + L (x2)				Standard: S (x2) + L (x2)				Standard: S (x2) + L (x2)				Standard: S (x2) + L (x2) Extra Long: S (x1) + L (x1)				Standard: S (x2) + L (x2)			
0.63	-0.03	Standard: S (x1) + L (x1)				Standard: S (x1) + L (x1)				Standard: S (x1) + L (x1)				Standard: S (x1) + L (x1)				Standard: S (x1) + L (x1)			

Table A2: Measured impact characteristics for all 54 regular wave tests with standard configuration.

Shorter Overhang - $W = 0.1$m																					
d [m]	R_c [m]	rAS				rBS				rCS				rDS				rES			
		I [Ns]	β [m]	t_d [ms]	Λ [-]	I [Ns]	β [m]	t_d [ms]	Λ [-]	I [Ns]	β [m]	t_d [ms]	Λ [-]	I [Ns]	β [m]	t_d [ms]	Λ [-]	I [Ns]	β [m]	t_d [ms]	Λ [-]
0.56	0.04	3.22	0.95	12	0.02	5.20	1.29	28	0.07	9.64	1.36	26	0.12	5.69	1.06	11	0.04	5.97	1.26	16	0.05
0.58	0.02	4.87	1.07	42	0.12	5.70	1.16	15	0.04	10.29	1.32	17	0.08	7.98	1.29	17	0.07	6.12	1.20	22	0.07
0.60	0.00	4.95	1.04	37	0.11	5.84	1.10	52	0.17	10.88	1.35	36	0.18	8.19	1.23	42	0.17	5.33	1.03	10	0.03
		4.89	1.09	38	0.11	5.36	1.09	59	0.18	10.00	1.29	33	0.16	7.62	1.22	46	0.18	5.50	1.11	16	0.05
		4.97	1.08	40	0.11													6.16	1.15	14	0.05
0.63	-0.03	0.00	-	-	-	6.25	1.31	89	0.26	11.78	1.60	67	0.30	7.54	1.21	56	0.22	4.77	0.94	90	0.28
Longer Overhang - $W = 0.2$m																					
d [m]	R_c [m]	rAL				rBL				rCL				rDL				rEL			
		I [Ns]	β [m]	t_d [ms]	Λ [-]	I [Ns]	β [m]	t_d [ms]	Λ [-]	I [Ns]	β [m]	t_d [ms]	Λ [-]	I [Ns]	β [m]	t_d [ms]	Λ [-]	I [Ns]	β [m]	t_d [ms]	Λ [-]
0.56	0.04	11.43	1.04	38	0.04	13.47	1.00	118	0.15	27.70	1.20	79	0.18	21.07	1.20	133	0.22	22.00	1.37	34	0.05
0.58	0.02	15.32	1.07	79	0.11	19.02	1.15	41	0.07	33.43	1.32	116	0.28	25.73	1.21	42	0.09	20.19	1.19	41	0.07
0.60	0.00	16.51	1.10	110	0.16	20.72	1.19	69	0.11	34.03	1.36	101	0.24	27.55	1.25	57	0.12	21.55	1.29	37	0.06
		15.19	1.06	114	0.16	20.11	1.27	91	0.14	30.82	1.28	98	0.23	23.94	1.18	68	0.13	21.90	1.35	40	0.06
		15.79	1.06	116	0.17													20.20	1.12	54	0.09
0.63	-0.03	0.00	-	-	-	17.58	1.18	158	0.23	20.56	0.91	37	0.08	23.98	1.24	90	0.17	20.87	1.28	95	0.15